NEW OBSERVATIONS OF THE INTERSTELLAR MEDIUM IN THE LYMAN BREAK GALAXY MS 1512−cB58 [1]

Max Pettini and Samantha A. Rix
Institute of Astronomy, Madingley Road, Cambridge, CB3 0HA, UK

Charles C. Steidel[2]
Palomar Observatory, Caltech 105–24, Pasadena, CA 91125

Kurt L. Adelberger[3]
Center for Astrophysics, 60 Garden Street, Cambridge, MA 02138

Matthew P. Hunt and Alice E. Shapley
Palomar Observatory, Caltech 105–24, Pasadena, CA 91125

[1]Based on data obtained at the W. M. Keck Observatory which is operated as a scientific partnership among the California Institute of Technology, the University of California, and NASA, and was made possible by the generous financial support of the W.M. Keck Foundation.

[2]Packard Fellow

[3]Harvard Society Junior Fellow

ABSTRACT

We present the results of a detailed study of the interstellar medium (ISM) of MS 1512−cB58, an $\sim L^*$ Lyman break galaxy at $z = 2.7276$, based on new spectral observations obtained with the Echelle Spectrograph and Imager on the Keck II telescope at 58 km s^{-1} resolution. We focus in particular on the chemical abundances and kinematics of the interstellar gas deduced from the analysis of 48 ultraviolet absorption lines, at rest wavelengths between 1134 and 2576 Å, due to elements from H to Zn. Our main findings are as follows. Even at this relatively early epoch, the ISM of this galaxy is already highly enriched in elements released by Type II supernovae; the abundances of O, Mg, Si, P, and S are all $\sim 2/5$ of their solar values. In contrast, N and the Fe-peak elements Mn, Fe, and Ni are underabundant by a factor of ~ 3. Based on current ideas of stellar nucleosynthesis, these results can be understood if most of the metal enrichment in cB58 has taken place within the last ~ 300 Myr, the timescale for the release of N from intermediate mass stars. Such a young age is consistent with the UV-optical spectral energy distribution. Thus, cB58 appears to be an example of a galaxy in the process of converting its gas into stars on a few dynamical timescales—quite possibly we are witnessing the formation of a galactic bulge or an elliptical galaxy. The energetic star formation activity has stirred the interstellar medium to high velocities; the strongest absorption lines span a velocity interval of ~ 1000 km s^{-1}. The net effect is a bulk outflow of the ISM at a speed of ~ 255 km s^{-1} and at a rate which exceeds the star formation rate. It is unclear whether this gas will be lost or retained by the galaxy. On the one hand, the outflow probably has sufficient energy to escape the potential well of cB58, for which we derive a baryonic mass of $\sim 10^{10} M_\odot$. On the other hand, at least some of the elements manufactured by previous generations of stars must have mixed efficiently with the ambient, neutral, ISM to give the high abundances we measure. We point out that the chemical and kinematic properties of cB58 are markedly different from those of most damped Lyman α systems at the same redshift.

Subject headings: cosmology: observations — galaxies: evolution — galaxies: starburst — galaxies: individual (MS 1512−cB58)

1. INTRODUCTION

Thanks to its gravitationally lensed nature, the $z = 2.7276$ galaxy MS 1512−cB58 (or cB58 for short) provides an unusually clear window on the population of star-forming galaxies identified at these redshifts through the Lyman break technique (Steidel et al. 1996). Discovered by Yee et al. (1996), cB58 is, as far as we can tell, a typical $\sim L^*$ galaxy magnified by a factor of ~ 30 by the foreground cluster MS 1512+36 at $z = 0.37$ (Seitz et al. 1998). This fortuitous alignment makes it by far the brightest known member of the Lyman break galaxy (LBG) population and has motivated a number of studies from mm to X-ray wavelengths (Frayer et al. 1997; Nakanishi et al. 1997; Baker et al. 2001; Sawicki 2001; Teplitz et al. 2000; Pettini et al. 2000a; Almaini et al., in preparation). In Pettini et al. (2000a, hereinafter Paper I) we described the main properties of the rest-frame ultraviolet spectrum of the galaxy; here we follow on that work with a more in-depth analysis made possible by the superior quality and wider wavelength coverage of recent spectroscopic observations with the Echelle Spectrograph and Imager (ESI) on the Keck II telescope. We focus in particular on the interstellar lines, which are fully resolved in the new data, with two main objectives. First, we consider the kinematics of the interstellar medium which show evidence for large scale outflows of gas and dust; such 'superwinds' are commonly observed in starburst galaxies at low and high redshifts (Heckman et al. 2000; Pettini et al. 2001), but have so far been little studied in the ultraviolet (UV) regime. Second, we shall attempt to deduce a comprehensive picture of the chemical composition of the interstellar gas, with the attendant clues which such information may provide on the evolutionary status of the galaxy and its past history of star formation. Abundance data for LBGs are still very patchy (Pettini 1999; Pettini et al. 2001 and references therein); apart from the opportunity to determine element abundances with some degree of confidence for the interstellar gas in cB58, we also hold the hope that the study of this unusually bright object may eventually lead us to identify some UV abundance indicators which can be applied more generally to the whole LBG population.

2. OBSERVATIONS AND DATA REDUCTION

ESI (Sheinis et al. 2000) is an efficient new instrument on the Keck II telescope; in its echelle mode it covers in a single 2048×4096 15μm pixel CCD frame the whole wavelength range from 4000 to 10 500 Å with 10 spectral orders at a dispersion of ~ 11.5 km s^{-1} per pixel. The current detector is an MIT/Lincoln Labs CCDID20 CCD which has a quantum efficiency greater than 70% from 4500 to nearly 8000 Å.

We observed cB58 with ESI on the nights of May 30, May 31 and June 1, 2000 for a total of 16 000 s ($8 \times 2\,000$ s exposures) in good conditions, with seeing between $0.65''$ and $0.85''$. We used a $1''$ wide entrance slit aligned at position angle PA = 93°, along the long axis of cB58 which is distorted into a gravitational fold arc approximately $3''$ long. All the observations were conducted

at airmass between 1.04 and 1.08 .

The ESI images were reduced, coadded and mapped onto a common vacuum heliocentric wavelength scale with the "Dukee" IRAF reduction package written by one us (KLA). Even for an extended object such as cB58, the minimum $20''$ separation between adjacent echelle orders provides adequate coverage of the sky background. Consequently, subtraction of the sky signal did not degrade significantly the signal-to-noise ratio and produced no obvious systematic error—that is, in the black cores of the strongest interstellar absorption lines we measured a mean count consistent with zero within the random noise. The one exception was the region near the damped Lyman α line in cB58 which, at $\lambda_{\rm obs} = 4527\,$Å, happens to fall close to the only serious CCD defect in the whole detector area. Here we applied a positive correction (that is, we *added* counts to raise the core of the line from negative flux values to zero), determined empirically and amounting to $\sim 7\%$ of the continuum level. Flux calibration was by reference to the spectra of the spectrophotometric standard stars Feige 34 and Feige 110 recorded on each night.

The final spectrum has a signal-to-noise ratio per resolution element of between ~ 30 and ~ 55 (the S/N varies along each echelle order) from ~ 4850 to $8750\,$Å ($\sim 1300 - 2350\,$Å in the rest-frame of cB58). From the widths of the night sky emission lines we measured a spectral resolution of $58\,{\rm km\ s^{-1}}$ FWHM.

3. THE INTERSTELLAR SPECTRUM OF MS 1512−cB58

3.1. The Systemic Redshift of the Galaxy

The ESI spectrum of cB58 exhibits a multitude of stellar and interstellar lines, as well as absorption from the Lyman α forest and several intervening metal line systems. Most of the stellar lines are blends from multiple transitions. The clearest single photospheric line is C III λ2296.871 (laboratory wavelength in air, corresponding to vacuum wavelength $\lambda_{\rm vac} = 2297.579$); we observe this line at a central wavelength $\lambda_{\rm obs} = 8564.4^{+0.2}_{-0.6}\,$Å from which we deduce a redshift $z_{\rm stars} = 2.7276^{+0.0001}_{-0.0003}$ (the asymmetric errors arise from a weak feature in the blue wing which may or may not be part of the line)[4]. Within the errors, this value is consistent with $z_{\rm stars} = 2.7268 \pm 0.0008$ derived in Paper I from a number of less well defined photospheric lines in the far-UV. Teplitz et al. (2000) measured $z_{\rm HII} = 2.7290 \pm 0.0007$ from the mean of ten emission lines formed in H II regions—from [O II] λ3727 to [N II] λ6583—redshifted into the near-infrared. It is unclear whether the 2σ difference between $z_{\rm HII}$ and $z_{\rm stars}$ reflects a real velocity offset of $\sim 100\,{\rm km\ s^{-1}}$ between the stars and the ionized gas, or is due to a systematic difference between the wavelength calibrations of the optical and infrared observations. In any case, here we adopt

[4]All redshifts quoted in this paper are vacuum heliocentric.

$z_{\rm stars} = 2.7276$ as the systemic redshift of cB58.

3.2. Interstellar Absorption Lines

Table 1 lists the interstellar absorption lines measured in our ESI spectrum of cB58. Together with Lyman α (not included in Table 1 but discussed separately in §4.1) we cover 48 transitions of elements from H to Zn in a variety of ionization stages, from neutral (H I, C I, O I, N I) to highly ionized species (Si IV, C IV, N V). Vacuum rest wavelengths and f-values of the transitions are from the compilation by Morton (1991) updated with subsequent revisions as listed by Savage & Sembach (1996) and R.F. Carswell (private communication). The interstellar lines are seen against the continuum provided by the integrated light of O and B stars in the galaxy. The resulting composite stellar spectrum is rich in photospheric and wind lines which are the subject of a future paper (see also Paper I). The resolution of the ESI data is adequate to allow, with some care, stellar and interstellar features to be separated in most cases; in this we are aided by the fact that the strongest interstellar absorption is centered at -255 km s^{-1} relative to the stellar redshift (§3.3). However, many of the interstellar lines at wavelengths below 1216 Å could not be recovered because they are blended with intervening Lyman α forest lines.

Rest-frame equivalent widths, W_0, are listed in column (6) of Table 1 together with their 1σ errors in column (7); they were measured by summing the absorption over fixed velocity ranges Δv indicated in column (5) of Table 1. The velocity ranges were chosen to encompass the full extent of the absorption while minimizing the amount of continuum included (and therefore the error on the equivalent width measurement); thus values of Δv are larger for the stronger lines. In a few cases (mostly in the Lyman α forest) where an interstellar line was found to be blended with other unrelated features over the interval Δv, we list its equivalent width as a lower limit which does not include the blend. Figures 1 and 2 are a compendium of absorption lines from different ionization stages of a variety of elements. We now describe the velocity structure of the absorbing gas.

3.3. Kinematics of the Absorbing Gas

The interstellar medium of cB58 has obviously been stirred and accelerated to high velocities, presumably by the kinetic energy deposited by the star formation activity via stellar winds and supernovae. The strongest transitions in Figures 1 and 2 show absorption over $\Delta v \sim 1000$ km s^{-1}, from ~ -775 to $\sim +225$ km s^{-1} relative to the redshift of the stars $z_{\rm stars} = 2.7276$. Gas with the largest optical depth occurs at velocities near $v_{\rm ISM} \simeq -255$ km s^{-1}, corresponding to an absorption redshift $z_{\rm abs} = 2.7244$. Thus the overall effect we are seeing is an outflow of the ISM from the star formation region. The outflow speed of -255 km s^{-1} is typical of Lyman break galaxies. It is now

well established that the *centroids* of the interstellar lines are normally blueshifted by between ~ 200 and $\sim 400\,\mathrm{km\ s^{-1}}$ relative to the emission lines from H II regions, at least in LBGs brighter than L^* (Pettini et al. 2001 and references therein). What the new observations presented here reveal is that there is gas in front of the stars with a much wider range of velocities, from ~ -500 to $\sim +500\,\mathrm{km\ s^{-1}}$, relative to the bulk of the outflow. We have no reason to believe that such extreme velocities are not commonly encountered in a significant fraction of LBGs, at least those whose spectra show strong interstellar absorption lines. At the low spectral resolution of most previous studies the velocity structure so evident here cannot be discerned, although the line equivalent widths themselves are indicative of values of Δv of several hundred km s^{-1} (Steidel et al. 1996).

Inspection of Figures 1 and 2 shows that all the ion stages observed have similar absorption profiles. First, they span the same overall velocity range, as can be realized by comparing, for example, Si II λ1526 in Figure 1 with the Si III and Si IV lines in Figure 2. Second, the gas with the highest optical depth is found at very similar velocities near $-255\,\mathrm{km\ s^{-1}}$; there is a shift of only $\sim 20\,\mathrm{km\ s^{-1}}$ between the neutrals and first ions ($v_{\tau\ \mathrm{max}} \simeq -265\,\mathrm{km\ s^{-1}}$; see Figure 1) and highly ionized species from Al III to N V ($v_{\tau\ \mathrm{max}} \simeq -245\,\mathrm{km\ s^{-1}}$; see Figure 2). The main difference between species which are the dominant ions in H I regions and those which trace ionized gas is that the latter show smoother absorption profiles. The Al III, Si IV and C IV doublets in Figure 2 are remarkable in their almost continuous decrease in optical depth over the interval $\pm 500\,\mathrm{km\ s^{-1}}$ from the central velocity of $-245\,\mathrm{km\ s^{-1}}$, while the first ions in Figure 1 break up into a number of seemingly discrete components.

The spatial and kinematic structure of the interstellar medium in cB58 is clearly very complex. Given the lack of detailed information, we can only speculate on the location and nature of the different absorption components. In the simplest picture, the starburst produces a large bubble of hot gas which sweeps out ambient interstellar matter as it expands and the main component of the absorption arises in compressed, cooling gas behind the shock front. Such a simple superbubble model can account for many (although not all) of the properties of the outflow seen in the local starburst galaxy NGC 1705 (Heckman et al. 2001b), but encounters some difficulties in the case of cB58. First, the cooling would have to be extremely efficient to give the high column densities of neutral gas we see (§4.1), since the high velocities imply shock temperatures $T = 2 \times 10^6 \times (v/300\,\mathrm{km\ s^{-1}})^2$ K, in the X-ray regime (Wallerstein & Silk 1971). Second, while the main absorption component centered near -255 km s^{-1}, which as we shall see below (§4.2) accounts for approximately two thirds of the column density of neutral gas, could in principle arise in such a supershell, the simple model provides no explanation for the rest of the absorption with $|\Delta v|$ of up to 500 km s^{-1} relative to it. Finally, a velocity of -255 km s^{-1} for the swept-up shell of interstellar matter appears rather high. The expansion speed of the shell is related to the rate of deposition of mechanical energy by the starburst, $\dot{E}_{42}$ (in units of 10^{42} erg s^{-1}), by the expression (e.g. Heckman 2001):

$$v_{\mathrm{shell}} \sim 100\,\dot{E}_{42}^{1/5}\,n_0^{-1/5}\,t_7^{-2/5}\,\mathrm{km\ s^{-1}} \qquad (1)$$

where n_0 is the ambient density and t_7 is the time since the expansion began in units of 10^7 years. From *Starburst99* (Leitherer et al. 1999) we find that the UV luminosity of cB58, $L_{1500} = 8 \times 10^{29}$ erg s^{-1} Hz^{-1} (corrected for gravitational lensing and dust extinction; see Paper I and references therein), corresponds to $\dot{E}_{42} = 32$. The spectral energy distribution of cB58 has been interpreted by Ellingson et al. (1996) and Bechtold et al. (1998) as evidence for an age $t_7 \lesssim 3.5$. From these parameters we would expect $v_{\rm shell} \simeq 120$ km s^{-1} for unity density of the ambient ISM. In order to reproduce the observed $v \simeq -255$ km s^{-1} we require either $n_0 \ll 1$ or $t_7 < 1$; while the former is a possibility, the latter seems unlikely because it would imply that we are viewing cB58 at a special time, soon after the onset of the starburst.

In an alternative scenario (see for example Strickland & Stevens 2000), the absorption arises *within* the cavity (filled with $T \sim 10^7$ K gas which is hard to observe directly) from fragments of the ambient ISM ablated by the hot gas. As these fragments are entrained in the flow they are accelerated from rest (relative to the stars) to speeds of up to ~ 750 km s^{-1} before they are heated and ionized to levels which are no longer observable with UV absorption line spectroscopy. While physically more plausible, this scenario does not naturally account for (a) the fact that most of the neutral gas is moving at $v = -265$ km s^{-1} relative to the stars, and (b) the similarity in the velocity profiles of absorption lines from different ionization stages, from species which are most abundant in neutral gas to the highly ionized Si IV and C IV. Naively, if the absorption arises from mass-loading of the flow, we would expect to see a progression towards more negative velocities with increasing ionization, as material is entrained and ionized by the ouflowing hot gas. This is the case in NGC 1705 (Heckman et al. 2001b). Possibly, such velocity differences are smeared and made difficult to recognize by the fact that we see absorption against an extended stellar background (see below), so that our spectrum is in fact the sum of many sightlines through the galaxy.

In any case, since the hydrodynamics of galactic superwinds are still poorly constrained, it is worthwhile pointing out here a few empirical considerations which should be accounted for in future theoretical treatments. First, there appears to be a high degree of symmetry in the kinematics of the outflow in cB58. Not only are the absorption profiles of different ionization stages broadly similar, as explained above, but the receding part of the outflow, which lies *behind* the stars and is detected via Lyman α emission (§4.1) also appears to exhibit essentially the same kinematics, mirroring at positive velocities the pattern seen in absorption. Given the stochastic nature of Lyman α emission, however, this could be no more than a coincidence—in other LBGs the peak of Lyman α emission is often at *higher* positive velocities than the blueshift of the absorption lines (see Figure 13 of Pettini et al. 2001). Second, whatever its location, the bulk of the gas moving at $v = -255$ km s^{-1} must be located well in front of the stars and cover them completely since it absorbs all of the UV light; as can be seen from Figures 1 and 2, the strongest metal absorption lines of all ion stages—from O I to C IV—are black at this velocity. From their detailed analysis of WFPC2 R and V images, Seitz et al. (1998) derived a source size $r_{1/2} = 0.25 \pm 0.05''$ (where $r_{1/2}$ is the half-light radius) which is magnified and distorted by

gravitational lensing into a gravitational fold arc about 3″ long and with an axis ratio of 1:7. A half-light radius of 0.25″ corresponds to linear dimensions $r_{1/2} = 2h_{70}^{-1}$ kpc for an $\Omega_M = 0.3$, $\Omega_\Lambda = 0.7$ cosmology; the structure responsible for the bulk of the absorption must therefore extend more than $2r_{1/2} = 4h_{70}^{-1}$ kpc across the line of sight. We return to the properties of the outflow in §6.3.

4. ION COLUMN DENSITIES

4.1. The Lyman α Line

As can be seen from Figure 3, the Lyman α line in cB58 is a combination of absorption and emission. The new data are fully consistent with the decomposition of this feature proposed in Paper I. The absorption component is best fitted by a damped profile with neutral hydrogen column density $N(\mathrm{H\ I}) = (7.0 \pm 1.5) \times 10^{20}\,\mathrm{cm}^{-2}$ centered at $v = -265\,\mathrm{km\ s}^{-1}$, the velocity where metal lines from species which are dominant ion stages in H I regions also have the largest optical depth. Superposed on the red wing of the damped absorption is an emission line with a characteristic shape (see bottom right-hand panel of Figure 3). The emission is strongest near $v \simeq +300\,\mathrm{km\ s}^{-1}$, is cut off abruptly on the blue side, and falls off more gradually at longer wavelengths. This composite absorption-emission profile of Lyman α conforms to the predictions for a line resonantly scattered in an expanding nebula (e.g. Tenorio-Tagle et al. 1999). The Lyman α photons we see are those back-scattered from outflowing material which lies *behind* the stars. Thus the emission mirrors the velocity structure seen in absorption in front of the stars; the agreement with the kinematics of the absorption lines described in §3.3 is very good. The tail of Lyman α emission extends to $v \sim +1000\,\mathrm{km\ s}^{-1}$, beyond the maximum velocity of $-750\,\mathrm{km\ s}^{-1}$ seen in absorption; presumably this extreme velocity gas, if it is also present in the approaching part of the outflow, has too low an optical depth in the metal lines covered by our spectrum to be detected in absorption.

4.2. Metal Lines

We derived values of column density N for ions of interest using two approaches. The first is the apparent optical depth method which is worth considering here, despite our relatively coarse resolution of $58\,\mathrm{km\ s}^{-1}$ FWHM, because the profiles of the absorption lines appear to be fully resolved. The apparent column density of an ion in each velocity bin, $N_a(v)$ in units of $\mathrm{cm}^{-2}\ (\mathrm{km\ s}^{-1})^{-1}$, is related to the apparent optical depth in that bin $\tau_a(v)$ by the expression

$$N_a(v) \;=\; \frac{\tau_a(v)}{f\lambda} \times \frac{m_e c}{\pi e^2} \;=\; \frac{\tau_a(v)}{f\lambda(\mathrm{\AA})} \times 3.768 \times 10^{14} \qquad (2)$$

where the symbols f, λ, c, e and m_e have their usual meanings. The apparent optical depth is deduced directly from the observed intensity in the line at velocity v, $I_{\rm obs}(v)$, by

$$\tau_a(v) \;=\; -\,ln\,[I_{\rm obs}(v)/I_0(v)] \tag{3}$$

where $I_0(v)$ is the intensity in the continuum. With the assumption of negligible smearing of the intrinsic line profile by the instrumental broadening function,

$$\tau_a(v) \approx \tau(v) \tag{4}$$

and the total column density of ion X, $N_{\rm aod}(X)$, is obtained by direct summation of eq. (2) over the velocity interval where line absorption takes place.

As emphasized by Savage & Sembach (1991), the attraction of the apparent optical depth method lies in the fact that no assumption has to be made concerning the velocity distribution of the absorbers. Furthermore, it provides a stringent consistency check when two or more transitions arising from the same atomic energy level, but with different values of the product $f\lambda$, are analyzed. The run of $N_a(v)$ with v should be the same, within the errors in $I_{\rm obs}(v)$, for all such lines. In general this condition will *not* be satisfied if there are unrecognized saturated components to the absorption lines; such a situation will manifest itself with the deduced value of $N_a(v)$ being smaller for lines with larger values of $f\lambda$. In our case a similar effect can also result from geometrical effects due to the fact that the background source against which the absorption takes place is not point-like, but is a spatially extended ensemble of O and B stars. If the covering of the integrated stellar continuum by the absorbing gas is inhomogeneous at a given velocity, the apparent optical depth method will give discordant values of column density for different transitions of the same ion at that velocity.

Values of $N_{\rm aod}$ deduced for absorption lines which are not saturated[5] are listed in column (5) of Table 2, while column (4) gives the velocity interval Δv over which equation (2) was summed. In Figures 4, 5, and 6 we have reproduced some examples of the run of $N_a(v)$ with v for lines of interest. Figure 4 shows the apparent optical depth profiles of the two ions for which we have the largest number of well-observed transitions, Fe II and Si II. The Fe II lines shown have values of $f\lambda$ spanning a range of a factor of 10, from the weakest λ2374 to the strongest λ2382, while from Si II λ1808 to Si II λ1260 the range in $f\lambda$ is a factor of 320. It can be seen from these plots that the absorption in the wings of the lines does not satisfy the consistency check discussed above, in that the value of $N(v)$ decreases with increasing $f\lambda$. As explained above, this could be an indication of either saturated absorption components which are too narrow to be resolved, or of inhomogeneous coverage of the stellar continuum. The situation is less clear-cut in the main component centered at $v = -265\,{\rm km\ s^{-1}}$. Here there is good agreement between Fe II λ2374 and λ1608 but these two lines differ by only a factor of 1.25 in their values of $f\lambda$. S II $\lambda\lambda 1250, 1253$

[5]Once $I_{\rm obs}(v)$ approaches zero, $\tau_a(v)$ becomes undetermined (see eq. 3) and the method is no longer applicable.

(Figure 5), with values of $f\lambda$ differing by a factor of 2, are also mutually consistent, although the weaker line is rather noisy.

The most suggestive evidence of inhomogeneous covering is provided by the Si IV doublet lines. As can be seen from the lower panel of Figure 6, the stronger member of the doublet consistently underestimates the column density at all velocities. The smoothness of the line profiles favors geometrical effects in the covering factor, rather than the presence of a multitude of regularly spaced, narrow, unresolved components, as the more likely interpretation. This would suggest that the *spatial* distribution of the ionized gas is significantly different from that of the neutral component (where the first ions of the heavy elements reside), even though both H II and H I gas occur over the same velocity interval. Al III appears to be an intermediate case (top panel of Figure 6).

Our second approach to the derivation of column densities consisted of fitting theoretical line profiles to only the central component of the absorption lines; this component accounts for most of the neutral gas to which our subsequent abundance analysis refers and, as argued above, geometrical covering factors may have only a secondary effect in the derivation of the column densities. We used the software package Xvoigt (Mar & Bailey 1995) to compute theoretical Voigt profiles, convolve them with the instrumental resolution, and compare them to the data. We found that all the Si II, S II, and Fe II lines could be fitted consistently (that is, with the same column density for all transitions of the same ion, irrespective of the value of $f\lambda$) with a single absorption component with velocity dispersion parameter $b = 70\,\mathrm{km\ s^{-1}}$ centered at $v = -265\,\mathrm{km\ s^{-1}}$. Furthermore, C I λ1157, the Mg II $\lambda\lambda$1239, 1240 doublet, P II λ1152, Mn II λ2576 (the strongest member of the triplet and the only one detected), and the numerous Ni II transitions are all consistent with these parameters, although they do not constrain them stringently because these weak features are generally noisy and in many cases blended (see Figure 7). The N I λ1134 and λ1199 triplets, which are intrinsically blended because the three lines are closer in wavelength than the velocity extent of the absorption, were also fitted with these values of b and v, and are discussed in more detail in §5.3 below.

Values of column density N_{pf} deduced by fitting the profile of the central component are listed in column (6) of Table 2. Comparison with the values of N_{aod} in column (5) shows that the former are consistently below the latter by 0.2 dex. That is, the central component accounts for 63% of the total column density observed. One exception is C I for which the two values of N are in good agreement; inspection of Figure 1 shows that this is because this line extends over a narrower velocity range than even the weakest lines from the first ions, and all the absorption is accounted for by a single $b = 70\,\mathrm{km\ s^{-1}}$ absorption component at $v = -265\,\mathrm{km\ s^{-1}}$.

5. ELEMENT ABUNDANCES

5.1. Which Column Densities?

We can summarize our column density determinations as follows. For all the species considered (except N I and Mg II which are discussed separately below), we cover at least one transition which is sufficiently weak for the apparent optical depth method to be applicable. The column densities derived this way have a typical statistical error of about ± 0.1 dex, but are systematically *underestimated* by an unknown amount because we see indications in the wings of the line profiles of either unresolved saturated components or inhomogeneous coverage of the integrated stellar UV light. Approximately two thirds of the column density is due to a main absorption component at $v = -265\,\mathrm{km\ s^{-1}}$ which apparently lies well in front of the stars and covers them completely, since the strongest absorption lines have black cores near this velocity.

We do not know what fraction of the total column density of neutral hydrogen resides in this component, as our estimate of $N(\mathrm{H\ I}) = 7.0 \times 10^{20}\,\mathrm{cm^{-2}}$ was derived by fitting the damping wings of the Lyman α line. However, this fraction is likely to be less than 100% because there is O I absorption at velocities beyond those attributable to the main component (see bottom right-hand panel of Figure 1).[6] Consequently, in deducing element abundances we have referred the *total* ion column densities to the above value of N(H I); the systematic error introduced by this assumption amounts to at most +0.2 dex (the ratio between the total column density of ion X and that due only to the component at $v = -265\,\mathrm{km\ s^{-1}}$).

Our estimate of N(H I) does not include any contribution from molecular hydrogen. Since our ESI spectrum does not extend to the far-UV wavelengths where the strongest H_2 transitions occur, we cannot place empirical limits on the molecular fraction of the gas. Qualitatively, it is likely that some H_2 is present in the main absorption component, where we see C I, because the same photons which would dissociate the H_2 molecules through absorption in the Lyman and Werner bands would also ionize C I (Hollenbach, Werner, & Salpeter 1971; Federman, Glassgold, & Kwan 1979). On the other hand, in local interstellar clouds with neutral hydrogen column densities comparable to that in cB58, the molecular fraction is seldom greater than 50%. For example, Savage et al. (1977) found $N(\mathrm{H\ I})/[N(\mathrm{H\ I}) + 2N(\mathrm{H_2})] \geq 0.5$ in all but two of the 109 stars they surveyed with the *Copernicus* satellite. A recent FUSE survey of 70 stars in the Small and Large Magellanic Clouds (Tumlinson et al. 2002) has shown that in the interstellar medium of those galaxies the molecular fraction is even lower. Thus, it would be surprising if the element abundances we deduce below were overestimates by more than a factor of two because of our inability to account for H_2, although obviously this uncertainty can only be resolved by extending the spectral study of cB58 to shorter wavelengths.

The values of N(X) adopted are listed in column (2) of Table 3; these are the same as the values of N_{aod} from Table 2 (with appropriate averaging when more than one line is available for

[6] O I and H I are closely tied together, so that $N(\mathrm{O\ I})/N(\mathrm{H\ I}) \simeq (\mathrm{O/H})$ irrespective of the ionized fraction of the gas (Sembach et al. 2000).

the same ion) with the exception of P II, N I, and Mg II. For P II we cover only one transition, at λ1152.818, which is blended with Lyman α forest absorption within the velocity range over which the optical depth is integrated; excluding this contamination we deduce log $N_{\rm aod} > 14.04$ (cm^{-2}). Profile fitting gives log $N_{\rm pf} = 14.00$ (cm^{-2}) for the main component only (see Figure 7); thus in Table 3 we have adopted log N(P II) = 14.20 (cm^{-2}) to account for the remainder of the absorption, as explained above. The situation is more complicated for N I and Mg II because the blending here is between lines of the same multiplet. When fitting the profiles of these blended features the wings from adjacent lines within the multiplet will have contributed somewhat to the absorption in the main component, and so it is unclear that the values of $N_{\rm pf}$ should in fact be corrected upwards by +0.2 dex in these cases too. We have not done so and adopted the values of $N_{\rm pf}$ in our abundance analysis; again the systematic error introduced is at most a factor of −0.2 dex and does not affect the main conclusions of our abundance analysis below.

5.2. Ionization Corrections

The species listed in Table 3 are the main ionization stages of their respective elements in H I regions; by taking the ratios of their column densities relative to N(H I) to give the abundances listed in column (3) we make the implicit assumption that the fractions of the first ions (and of N I) which reside in ionized gas are negligible for our purposes. At first sight there may seem to be little justification for this assumption—after all we know from our data that there is ionized gas at the same velocities as the neutrals and first ions (Figures 1 and 2).

The problem of correcting interstellar abundance measurements for H II region 'contamination' is not a new one (e.g. Steigman, Strittmatter, & Williams 1975); most recently it has been scrutinized in detail by Howk & Sembach (1999) and Vladilo et al. (2001) using the CLOUDY code (Ferland et al. 1998). Vladilo et al. have specifically calculated the relevant corrections as a function of neutral hydrogen column density, prompted by the realization that in damped Lyman α systems (DLAs) highly ionized species—particularly Al III—are often coincident in velocity with the first ions, as is the case here. These authors confirm the main conclusion of previous work, that the corrections to interstellar abundances due to the presence of ionized gas along the line of sight are generally small. For the elements considered here, when log N(H I)= 20.85 (cm^{-2}) as in cB58, the largest correction is for P II with log (P/H) = log [N(P II)/N(H I)] − 0.1 dex.

What the CLOUDY calculations show is that when ionizing radiation impinges on the surface of a neutral interstellar cloud and ionizes its outer layer, this H II region contains relatively small fractions of the first ions compared with the interior, self-shielded, H I region (at least when N(H I) $\gtrsim 2 \times 10^{20}$ cm^{-2}), because higher ionization stages than the first ions dominate. The situation under consideration here is more complex than that considered by Vladilo et al. (2001) whose calculations did not include processes such as X-ray ionization from the very high temperature gas which presumably drives the outward motion of the ISM in cB58, nor the conduction between the expanding bubble of hot gas and the swept-up interstellar matter. Even

so, it is unlikely that these additional sources of ionization would affect significantly the relative abundances of the neutrals and first ions. On the other hand, ionization corrections may be important if the column density $N(\mathrm{H\ I}) = 7.0 \times 10^{20}$ cm^{-2} we measure in cB58 is due to the superposition of many individual components, each with $N(\mathrm{H\ I}) < 1 \times 10^{20}$ cm^{-2}.

5.3. Chemical Abundances in the Interstellar Medium of cB58

In summary, we have examined various sources of systematic uncertainty which could affect the abundance determinations in Table 3 and concluded that in general these are likely to be less than 0.2 dex. We have no way of quantifying the effect of saturation in the wings of the line profiles which may have caused us to underestimate the overall level of metallicity; in order to do so we have to rely on comparing our results with what is already known about the degree of metal enrichment of cB58. The last column in Table 3 gives the abundances of the elements observed relative to the solar reference scale; these are also shown graphically in the top panel of Figure 8. We now discuss these results individually.

Our observations cover three α-capture elements, Mg, Si, and S; all three give a consistent picture with abundances approximately 2/5 solar or $[\mathrm{Mg,Si,S/H}]_{\mathrm{cB58}} \simeq -0.4$ in the usual notation. This is in excellent agreement with the value $[\mathrm{O/H}]_{\mathrm{cB58}} \simeq -0.35$ for the *ionized* gas, obtained by Teplitz et al. (2000) from infrared observations of nebular emission lines.[7] The agreement, unless entirely fortuitous, gives confidence in our abundance analysis and shows that the systematic uncertainties discussed at length above have not been underestimated in our treatment. The abundance of P, $[\mathrm{P/H}]_{\mathrm{cB58}} \simeq -0.21$, is in line with those of Mg, Si, and S, given the errors.

Nitrogen, on the other hand, is apparently ten times less abundant than the α elements relative to the solar scale, and ~ 3 times below the typical $\log(\mathrm{N/O}) = -1.35$ measured in nearby galaxies when $[\mathrm{O/H}] = -0.35$ (Henry, Edmunds, & Köppen 2000).[8] The low abundance of N we derive contrasts with the results of the nebular analysis by Teplitz et al. (2000). These authors used their measurement of the [N II]/[O II] ratio to deduce $\log(\mathrm{N/O}) = -1.24$ or $[\mathrm{N/H}]_{\mathrm{cB58}} \simeq -0.78$, whereas we find $[\mathrm{N/H}]_{\mathrm{cB58}} \simeq -1.43$, a difference of a factor of 4.5. To explore the origin of this discrepancy we used Xvoigt to compute the absorption profiles of the N I λ1134 (see Figure 9) and λ1199 triplets produced by the main absorption component of the interstellar lines at $v = -265$ km s^{-1} with $b = 70$ km s^{-1} and $N(\mathrm{N\ I}) = 1.0 \times 10^{16}$ cm^{-2}, the column density of N I corresponding to the value $[\mathrm{N/H}]_{\mathrm{cB58}} \simeq -0.78$ derived by Teplitz et al. (2000). As can be

[7]Using the ratio of [O II] and [O III] to Hβ (the R_{23} method of Pagel et al. 1979), Teplitz et al. found $\log(\mathrm{O/H}) \simeq -3.61$. With the recent revision of the solar oxygen abundance proposed by Holweger (2001), $\log(\mathrm{O/H})_{\odot} = -3.26$, this leads to $[\mathrm{O/H}]_{\mathrm{cB58}} \simeq -0.35$.

[8]For comparison, $\log(\mathrm{N/O})_{\odot} = -0.81$ (Holweger 2001). The dependence of (N/O) on [O/H] results from the complex nucleosynthesis of N, which has both a primary and a secondary component—see the discussion by Henry et al. (2000).

seen from Figure 9, such a high value of N I is highly inconsistent with our absorption line data.

We have considered a number of possible explanations for the difference in the N abundance deduced from absorption and emission line measurements. First, the conversion from the emission line ratios to (N/O) has only a minor temperature dependence which cannot account for the factor of 4.5 discrepancy. Second, the possibility that there is a real composition difference between ionized and neutral gas seems unlikely because (a) there are no precedents for such abundance inhomogeneities in local galaxies (Meyer, Cardelli, & Sofia 1997; Esteban et al. 1998; Kobulnicky 1999), and (b) the abundances of the α elements Mg, Si, and S we derive for the neutral component are all in excellent agreement with that of O in the H II gas. Third, one may conjecture that N may be more highly ionized than H, if the H I region is permeated by extreme ultraviolet photons produced from stars and hot gas, since the cross section for photoionization of N I to N II is higher than that of H I. Such ionization effects have been considered in detail by Sofia & Jenkins (1998) and Jenkins et al. (2000) who found them to be important only when $N(\mathrm{H\ I}) \lesssim 10^{19}\,\mathrm{cm}^{-2}$, that is at column densities of neutral hydrogen ~ 100 times lower than that seen in cB58. When $N(\mathrm{H\ I}) > 10^{20}\,\mathrm{cm}^{-2}$, the interstellar ratio N I/H I is in good agreement with the solar abundance of N (Sofia & Meyer 2001a,b). In the nearby starburst galaxy NGC 1705, where $N(\mathrm{H\ I}) \simeq 1.5 \times 10^{20}\,\mathrm{cm}^{-2}$, Heckman et al. (2001b) were able to address this point directly with observations of both N I and N II, and indeed they found that N I/N II $\simeq$ H I/H II. We conclude that ionization effects are unlikely to have led us to underestimate significantly the abundance of N in our absorption line analysis.

On the other hand, examining the NIRSPEC spectra published by Teplitz et al. (see their Figure 3), it can be realized that the weak [N II] $\lambda\lambda 6548, 6583$ lines are right at the edge of their data and, at observed wavelengths of 2.44204 and 2.45566 μm respectively, well beyond the conventional boundary of the K-band window, in a region where both atmospheric absorption and thermal emission are high. It is conceivable, therefore, that their fluxes may have been overestimated; the problem is compounded by the awkward location of [O II] $\lambda 3727$ ($\lambda_{\mathrm{obs}} = 1.3898\,\mu$m) between the J and H windows, close to the maximum of H_2O absorption at these wavelengths. It is also true that among our abundance determinations that of N is the least precise, because the individual lines in the two triplets are not resolved, but any additional absorption components which have been omitted in the profile fit shown in Figure 9 would probably have the net effect of reducing, rather than increasing the value of N(N I).

Turning to the Fe-peak group, we have abundance measurements for three elements, Mn, Fe, and Ni. As can be seen from Figure 8, they are all less abundant than S and the other α-capture elements, by factors of between 0.4 (Ni) and 0.75 (Fe) dex. This could be a real departure from the solar scale, or a reflection of the common depletions of Mn, Fe, and Ni onto dust grains, or both. The ambiguity could in principle be resolved by consideration of the abundance of Zn, an iron-peak element which is normally undepleted (e.g. Pettini, Boksenberg, & Hunstead 1990). Unfortunately, we cannot derive a useful measure of [Zn/H] because the Zn II doublet lines are blended with atmospheric B-band absorption and with stellar photospheric lines.

We can still explore this question in a less direct way by comparing the pattern of element abundances in cB58 with that of the interstellar gas near the Sun as reviewed by Sembach & Savage (1996) and Savage & Sembach (1996). These authors give illustrative cases of the depletions of refractory elements observed in different interstellar environments, from diffuse, cool clouds in the disk (where the depletions are most pronounced) to low-density halo sight-lines (where depletions are less severe). In Figure 8 we compare the pattern of abundances in cB58 (top panel) with that typically found along Galactic sight-lines which intercept warm clouds in the disk and halo (lower panel).[9] To facilitate the comparison, we show the Galactic measures (thin rectangles) shifted to lower values by the -0.40 dex intrinsic underabundance of the α-elements in cB58 (thick rectangles). The relative abundance of Ni in the lower panel of Figure 8 has been increased by 0.27 dex to account for the downward revision of the f-values of the relevant transitions (Fedchak, Wiese, & Lawler 2000 and references therein) since the compilation by Savage & Sembach (1996). The abundances of N and P, not included in the compilation by Savage & Sembach, are from the surveys by Meyer et al. (1997) and Dufton, Keenan, & Hibbert (1986) respectively.

From the lower panel of Figure 8 it can be realised that, if depletion were the sole origin of the observed underabundances of the Fe-peak elements in cB58 (relative to the undepleted S), then we would also expect Mg, Si, and P to be depleted, albeit to a lesser degree. This is not what is observed in cB58 (top panel), where all three elements are approximately solar relative to S. Of course there is no reason why the composition of dust grains in the compressed, outflowing, ISM of cB58 should be the same as that seen in nearby Galactic clouds. Furthermore, some dust *must* be present in the ISM of cB58, since the UV continuum is significantly reddened (Paper I) and dust emission has been detected directly at sub-mm and mm wavelengths (van der Werf et al. 2000; Baker et al. 2001). On the other hand, the fact that all the observed Fe-peak elements are uniformly below the α-capture group—coupled with the obviously instrinsic (i.e. not due to dust depletion) underabundance of N—is very suggestive of more fundamental differences between this high redshift galaxy and the Milky Way in their histories of element production, as we now discuss. The most likely scenario, in our view, is that both dust depletion and intrinsic departures from the solar scale contribute to the pattern of element abundances we have uncovered in cB58.

6. DISCUSSION

6.1. The Star Formation History of cB58

What do these results tell us about the history of star formation in cB58? The most immediate and straightforward conclusion is that this galaxy had already achieved a near-solar metallicity

[9]We have chosen this example simply because the deficiency of Fe is similar to that found in cB58 and data are available for several elements. Our conclusion would still be the same if we compared with one of the other Galactic depletion patterns which roughly match the Fe abundance in cB58.

at relatively early times, some 12 Gyr ago in a $\Omega_M = 0.3$, $\Omega_\Lambda = 0.7$, $h = 0.65$ cosmology, when the age of the universe was only 17% of what it is today. The results of our quantitative analysis of the interstellar absorption lines confirm earlier inferences of a high metallicity based on the strengths of the stellar wind lines, which exhibit P Cygni profiles of comparable extent to those seen in O stars of the Large Magellanic Cloud (Paper I; Leitherer et al. 2001). The advanced degree of chemical enrichment we have established is consistent with the original suggestion by Steidel et al. (1996) that, in the Lyman break galaxies, we see the progenitors of today's ellipticals and bulges, and with a general prediction of hydrodynamic cosmological simulations (e.g. Cen & Ostriker 1999; Nagamine et al. 2001) which show that such relatively high abundances are in fact common in the most massive galaxies at $z \simeq 3$. Of course we do not know whether in this respect cB58 is typical of the Lyman break galaxy population in general. However, its nebular emission line ratios *are* very much in line with those of other L^* LBGs studied by Pettini et al. (2001). In that paper we showed how the R_{23} values measured admit a range of values of [O/H], because of the double-valued nature of this abundance calibrator. If cB58 is a typical member of the sample, solutions on the upper branch of the R_{23} vs. [O/H] relation are favored, corresponding to near-solar abundances of oxygen.

The second conclusion from the present study is that elements whose release into the ISM is delayed relative to the α-capture products of Type II supernovae are significantly underabundant in cB58. The most obvious example is N for which dust depletion is not an issue, but we have argued that even the refractory Fe-peak elements probably exhibit a degree of intrinsic deficiency relative to the solar pattern of abundances. In standard chemical evolution models, intermediate mass stars are the main source of N, while Type Ia supernovae contribute most of the Fe-peak elements. In both cases the evolutionary times are significantly longer than the near-instantaneous cycling by massive stars which explode as Type II supernovae, with the consequence that the mixing of N and Fe-group elements into the ISM is delayed by between 300 Myr and 1 Gyr.[10]

The results of our analysis would then suggest a relatively young age for cB58. Ellingson et al. (1996) reached a similar conclusion by fitting the rest-frame UV-optical spectral energy distribution (SED) of the galaxy with spectral synthesis models, favouring an age of less than 35 Myr. However, this only applies to the stellar population responsible for most of the UV-optical light we see; longer wavelength photometry would be required to recognize an older population which has now 'switched-off', even if it accounted for as much as 90% of the galaxy mass. This is a common limitation in the diagnostic value of SEDs when only a relatively narrow range of wavelengths is available (e.g. Papovich, Dickinson, & Ferguson 2001). The abundance data presented here, on the other hand, when interpreted in the context of current ideas of stellar nucleosynthesis, rule out the existence of a significant population of stars older than ~ 300 Myr—had such an earlier episode

[10] An alternative way to reduce the relative abundances of elements synthesized by intermediate mass stars is to appeal to a top heavy, or truncated, initial mass function (IMF). Although we cannot exclude this possibility, we consider it less likely, given the lack of positive evidence to date against the simplest assumption of a universal IMF (Kennicutt 1998; Feltzing, Gilmore, & Wyse 1999; Molaro et al. 2001).

of star formation taken place, it would have enriched the ISM of cB58 in N above the observed level. Unpublished *ISOCAM* photometry, covering the rest frame near-IR region from 1 to 4 μm, is consistent with this picture; in their preliminary conference report Bechtold et al. (1998) place an upper limit of $\sim 10\%$ to the fraction of the stellar mass contributed by a 2 Gyr-old population.

The spectral character of cB58—with its reddened UV continuum, strong saturated interstellar lines, and very weak Lyman α emission—fits in well with the scenario proposed by Shapley et al. (2001) where these are precisely the youngest galaxies in the Lyman break population. Thus, *in cB58 we may well have an empirical example of a galaxy caught in the act of converting a substantial fraction of its interstellar gas into stars on a few dynamical timescales.* Incidentally, our value of [N/α] resolves the apparent discrepancy noted by Teplitz et al. (2000) between the relatively high (N/O) they derived and the young age deduced by Ellingson et al. (1996). Precise abundance determinations from weak nebular emission lines are difficult once these features are redshifted into the near-IR, as is the case in LBGs. Such work will probably have to await the availability of the Next Generation Space Telescope to develop fully.

6.2. Comparison with Damped Lyman α Systems

The pattern of element abundances in Figure 8 is strikingly different from that typical of damped Lyman α systems. First, DLAs at all redshifts are generally metal poor and the chance of finding one with metallicity $Z_{\rm DLA} \simeq 2/5 Z_{\odot}$ at redshifts $z = 2 - 3$ is only about one in ten (Pettini et al. 1999). Second, and somewhat paradoxically, the enhancement of the α-elements relative to Fe *expected* at these low metallicities by analogy with metal-poor stars in the Milky Way has proved very elusive to pin-down in DLAs (Vladilo 1998; Pettini et al. 2000b; Prochaska & Wolfe 2002). The data for N are less extensive, but again the majority of DLAs seem to have (N/O) ratios in line with those of today's metal-poor galaxies where there has been sufficient time for the dispersal of the primary N from stars of intermediate mass (Henry et al. 2000; Lattanzio et al., in preparation).

There are also obvious differences in the kinematics of the absorbing gas between DLAs and cB58. Metal lines seldom span more than 300 km s^{-1} in damped systems (Prochaska et al. 2001), whereas we have found that in cB58 the same transitions extend over an interval $\Delta v \simeq 1000$ km s^{-1}. Furthermore, while all ion stages observed in cB58 broadly share the same velocity structure, this is not generally the case in DLAs. Here it is common to find significant differences in the kinematics of high and low ions; Wolfe & Prochaska (2000) have taken this as evidence for distinct sub-structures, such as infalling ionized clouds and a neutral thick disk, within the same dark matter halo.

These chemical and kinematic differences can be understood if star formation proceeds at a much faster pace in LBGs compared with the DLAs, and indeed several recent theoretical studies have proposed such a picture (e.g. Mo, Mao, & White 1999; Jimenez, Bowen, & Matteucci 1999).

What is surprising, perhaps, is that there should be so little overlap between the properties of these two populations (as far as we can tell on the basis of the available, limited, set of data), almost as if their modes of star formation were qualitatively different.

6.3. Outflows in Lyman Break Galaxies

As we have seen, the bulk of the ISM of cB58, rich in the accumulated products of stellar nucleosynthesis, is moving outwards from the star forming region with a velocity $v \simeq 255\,\mathrm{km\ s^{-1}}$; furthermore, there is gas with outflow speeds up to $3-4$ times higher seen both in interstellar absorption and Lyman α emission. In Paper I we showed that, if the column density N is confined to a spherically symmetric thin shell of radius d expanding with velocity v, the implied mass outflow rate is

$$\dot{M} \sim 70 \times \left(\frac{d}{1\ \mathrm{kpc}}\right) \times \left(\frac{N}{7\times10^{20}\ \mathrm{cm^{-2}}}\right) \times \left(\frac{v}{255\ \mathrm{km\ s^{-1}}}\right)\ M_\odot\ \mathrm{yr^{-1}}. \tag{5}$$

We also pointed out that this value is comparable to the star formation rate $\mathrm{SFR} \simeq 40 M_\odot\ \mathrm{yr^{-1}}$ deduced from the far-UV luminosity L_{1500} after correcting for a factor of ~ 7 attenuation by dust extinction. While we have no direct information on the dimensions of the shell, the fact that the absorbing material seems to cover completely the stars suggests that d may well be $> 1\,\mathrm{kpc}$. As mentioned in §3.3, the lensing analysis by Seitz et al. (1998) favoured a source size $r_{1/2} = 2h_{70}^{-1}\,\mathrm{kpc}$, where $r_{1/2}$ is the half-light radius in the rest-frame UV; if $d \gtrsim 2r$, $\dot{M}$ in equation (5) may well be many times greater than the SFR, unless we are seeing a highly collimated outflow. This conclusion would be further strengthened by including in the calculation the higher velocity gas, if its ionized fraction is high so that $N(\mathrm{H\ II}) > N(\mathrm{H\ I})$ at $v \gg 255\ \mathrm{km\ s^{-1}}$.

Such powerful superwinds are seemingly common in LBGs—the $255\,\mathrm{km\ s^{-1}}$ blueshift of the interstellar lines in cB58 is certainly typical of the sample of LBGs with luminosities $L \geq L^*$ (Pettini et al. 2001; Adelberger et al., in preparation). Comparable outflows are seen in local starburst galaxies when the star formation rate per unit area exceeds $0.1 M_\odot\ \mathrm{yr^{-1}\ kpc^{-2}}$ (Heckman et al. 2000). At both high and low redshifts the impact of these outflows on their host galaxies and on the surrounding environment must be considerable. Quantitatively, an important question is whether the superwinds and the material entrained in the flow escape the galaxies altogether or remained confined within their gravitational potential wells. Aguirre et al. (2001) have, among others, addressed this question with the aid of hydrodynamical simulations and concluded that the most important factors determining the stall radius of the shell are the wind velocity, the mass of the wind-driving galaxy, and the fraction of ambient ISM entrained.

We can roughly estimate the mass of cB58 as follows. Under the simplest assumption that the star formation rate has remained constant for a period between ~ 30 and $\sim 300\,\mathrm{Myr}$, the formed stellar mass is

$$m_{\mathrm{star}} \simeq 4\times10^9\, t_{\mathrm{sf8}}\, M_\odot \tag{6}$$

where $t_{\rm sf8}$ is the duration of the star formation activity in units of 100 Myr. In order to reach a metallicity $Z \simeq 2/5 Z_\odot$, at least 1/3 of the gas reservoir must have been processed into stars (for a solar yield; Edmunds 1990). Thus,

$$m_{\rm baryons} \lesssim 1.2 \times 10^{10}\, t_{\rm sf8}\, M_\odot \tag{7}$$

This is comparable to the dynamical mass

$$m_{\rm dyn} \simeq 1.3 \times 10^{10}\, M_\odot \tag{8}$$

for the starburst region obtained by substituting into the expression

$$m_{\rm dyn} = 1.2 \times 10^{10} M_\odot \left(\frac{\sigma}{100\,{\rm km\ s^{-1}}} \right)^2 \frac{r_{1/2}}{\rm kpc} \tag{9}$$

(Pettini et al. 2001) the velocity dispersion of the nebular emission lines $\sigma = 81\,{\rm km\ s^{-1}}$ measured by Teplitz et al. (2000) and $r_{1/2} = 2h_{70}^{-1}$ deduced by Seitz et al. (1998).

The simulations by Aguirre et al. (2001) predict that for masses of order $10^{10}\,M_\odot$ and *initial* outflow speeds of $\sim 300\,{\rm km\ s^{-1}}$ the stall radius is relatively small, $r_{\rm stall} \lesssim 10\,{\rm kpc}$. However, if the absorbing gas we see moving at $v = -255$ km s^{-1} is located several kpc in front of the stars, as we have argued above, then (a) its initial velocity must have been significantly higher, and (b) it has already climbed out of much of the potential well. For example, the escape velocity from $d = 4\,{\rm kpc}$ within a Navarro, Frenk, & White (1997) halo of mass 10^{10} (10^{11}) $M_\odot$ is ~ 140 (~ 350) km s^{-1} (Adelberger et al., in preparation), well within the velocities we measure. Empirically, we can only say that cB58 must have been able to retain at least some—if not most—of the heavy elements synthesized by earlier star formation episodes, given that we now see them mixed in the ambient, neutral ISM.

More generally, however, the work by Adelberger et al. (in preparation) show that outflows from LBGs have a detectable impact on the intergalactic medium (IGM) out to large radii, of order 100 kpc. Together with the wide range of ages of LBGs deduced by Shapley et al. (2001), these results may help explain the presence of metals in the Lyman α forest up to highest redshifts probed ($z = 5$; Songaila 2001). This raises an interesting possibility. If the rapid processing of gas into stars we have found in cB58 were common to most LBGs, it is possible that, in at least some cases, the gas polluting the IGM has a distinctly non-solar composition, with a relative deficiency of the elements synthesized by intermediate and low mass stars. While there are clues that N may indeed be underabundant relative to C and Si in the Lyman α forest at $z > 3$, (Boksenberg & Sargent, in preparation), in general it is difficult to distinguish abundance anomalies from other factors, such as the shape of the ionizing radiation field, which contribute to the relative column densities of the few ion stages observed in the forest.

Finally, the impact of violent star formation on the ambient ISM of cB58 will not be limited to kinematic effects. It is also likely to produce regions where the gas is optically thin to Lyman continuum photons which can thus escape into the IGM and contribute to the ionizing background

(Steidel, Pettini, & Adelberger 2001). Heckman et al. (2001a) have recently used the example of cB58 to argue that superwinds do not necessarily clear out such channels, by pointing out that if the metal lines are optically thick in their cores, the optical depth at the Lyman edge is likely to be orders of magnitude larger. Indeed, on the basis of the results presented here, we would not expect to detect any flux below 912 Å in cB58; although we argued earlier that the covering factor of some absorption components may not be unity, there is little doubt that the bulk of the ISM moving at $v = -255$ km s^{-1} is opaque to ionizing radiation *as viewed from our line of sight*. Nevertheless, this does not preclude the possibility that the UV light from O and B stars may be escaping in other directions. A local example is provided by NGC 1705 where the strongest interstellar absorption lines have black cores, and yet there is evidence that the superbubble created by the starburst has begun to break out of the galaxy and fragment, allowing the hot interior gas to vent out into the IGM (Heckman et al. 2001b).

7. SUMMARY AND CONCLUSIONS

We have presented our analysis of the interstellar spectrum of MS 1512−cB58, an L^* Lyman break galaxy at $z = 2.7276$ which is undergoing active star formation at a rate of $\sim 40 M_\odot$ yr^{-1}. The observations, which have a spectral resolution of 58 km s^{-1}, have been made possible by the gravitationally lensed nature of cB58 and the high efficiency of the new Echelle Spectrograph and Imager on the Keck II telescope. Our main findings are as follows.

1. The ambient interstellar medium of cB58 is highly enriched in the chemical elements released by Type II supernovae; O, Mg, Si, P, and S all have abundances of $\sim 2/5$ solar. Thus, even at this relatively early epoch (corresponding to a look-back time of 83% of the age of the universe in today's favored cosmology), this galaxy had already processed at least one third of its gas into stars.

2. The galaxy appears to be chemically young, in that it is relatively deficient in elements produced by intermediate mass stars whose evolutionary timescales are longer than those of Type II supernova progenitors. N and the Fe-peak elements we observe (Mn, Fe, and Ni) are all less abundant than expected by factors between 0.4 and 0.75 dex. Depletion onto dust, which is known to be present in cB58, probably accounts for some of the Fe-peak element underabundances, but this is not likely to be an important effect for N. On the basis of current ideas of the nucleosynthesis of N, it would appear that much of the ISM enrichment in cB58 has taken place within the last 300 Myr, the lifetime of the intermediate mass stars believed to be the main source of N. For comparison, the starburst episode responsible for the UV and optical light we see is estimated to be younger than ~ 35 Myr, on the basis of theoretical models of the spectral energy distribution at these wavelengths.

3. Taken together, these two findings are highly suggestive of a galaxy caught in the act of

converting its interstellar medium into stars on a few dynamical timescales—quite possibly in cB58 we are witnessing the formation of a galactic bulge or an elliptical galaxy. The results of our chemical analysis are consistent with the scenario proposed by Shapley et al. (2001), whereby galaxies whose UV spectra are dominated by strong, blueshifted, absorption lines, as is the case here, are at the young end of the range of ages of LBGs. Our findings also lend support to models of structure formation which predict that, even at $z \simeq 3$, near-solar metallicities should in fact be common in galaxies with masses greater than $\sim 10^{10} M_{\odot}$ (e.g. Nagamine et al. 2001). For cB58 we deduce a baryonic mass $m_{\rm baryons} \simeq 1 \times 10^{10} M_{\odot}$, from consideration of its star formation history, metallicity, and velocity dispersion of the ionized gas.

4. The chemical properties of cB58 are markedly different from those of most damped Lyman α systems at the same redshift. DLAs are significantly less metal-rich, typically by about one order of magnitude, and seldom exhibit the enhancement of the α-capture elements we have uncovered here. Presumably star formation is a slower and more protracted process in DLAs than in LBGs, again consistent with current theoretical ideas about these two populations of high redshift galaxies.

5. The interstellar medium in cB58 has been stirred to high velocities by the energetic star formation activity. In the strongest metal transitions, absorption extends over a velocity interval of ~ 1000 km s^{-1}. The net effect is an outflow of the bulk of the ISM at a speed of ~ 255 km s^{-1} which we see both in absorption in front of the stars and in emission of Lyman α photons back-scattered from gas behind the stars. There seems to be a high degree of symmetry in the kinematics of approaching and receding portions of the flow; this and other empirical properties we have delineated will provide constraints to future modeling of such superwinds from starburst galaxies.

6. Unless the outflow is highly collimated, the mass outflow rate exceeds the star formation rate. It is unclear whether the outflowing gas is still bound to the galaxy. We suspect that its velocity exceeds the escape velocity within the potential well of cB58 but, on the other hand, the high metallicity of the ambient ISM suggests that most of the elements synthesized by previous generations of stars have been retained. In general, outflows from LBGs seem the likely source of at least some of the metals present in the Lyman α forest up to the highest redshifts probed. Although the ISM of cB58 is optically thick to Lyman continuum photons along our line of sight, there remains the possibility that ionizing photons are leaking out of the galaxy in other directions, through channels cleared out in the highly disturbed interstellar medium.

While we have made some progress in measuring some of the physical parameters of this Lyman break galaxy, we remain acutely aware of the fact that we are dealing with a single object. How typical is cB58 of the Lyman break population as a whole? There are indications that some of the above results, particularly the high metallicity, the rapid star formation timescale, and the kinematics of the outflow, may well be common to at least a subset of LBGs (Pettini et al. 2001; Shapley et al. 2001). However, extending the detailed analysis presented here to other high

redshift galaxies, targeting a variety of spectral morphologies, remains a high priority for future work. Obviously there is a strong incentive to identify further cases of gravitationally lensed LBGs, but few sources will be as favorably located relative to the lens as cB58. Possibly the stellar, rather than interstellar, spectrum will provide the means to study the chemical abundances and other properties of Lyman break galaxies in a more wholesale manner; we intend to address this question in a future paper.

We are grateful to the ESI team for providing us with the efficient instrument which made this study possible, and to the staff of the Keck Observatory for their competent assistance with the observations. We are indebted to Ken Sembach for many suggestions which improved the paper significantly, and to Andrew Baker, Martin Haehnelt, Tim Heckman, Francesca Matteucci, and Jeremiah Ostriker for valuable discussions. CCS, KLA, MPH, and AES have been supported by grants AST95-96229 and AST-0070773 from the U.S. National Science Foundation, and by the David and Lucile Packard Foundation. Finally, we wish to extend special thanks to those of Hawaiian ancestry on whose sacred mountain we are privileged to be guests. Without their generous hospitality, the observations presented herein would not have been possible.

REFERENCES

Aguirre, A., Hernquist, L., Schaye, J., Weinberg, D.H., Katz, N., & Gardner, J. 2001, ApJ, 560, 599

Baker, A. J., Lutz, D., Genzel, R., Tacconi, L. J., & Lehnert, M. D. 2001, A&A, 372, L37

Bechtold, J., Elston, R., Yee, H.K.C., Ellingson, E., & Cutri, R.M. 1998, in ASP Conf. Ser. 146, The Young Universe, ed. S. D'Odorico, A. Fontana, & E. Giallongo (San Francisco: ASP), 241

Cen, R., & Ostriker, J.P. 1999, ApJ, 519, L109

Dufton, P.L., Keenan, F.P., & Hibbert, A. 1986, A&A, 164, 179

Edmunds, M.G. 1990, MNRAS, 246, 678

Ellingson, E., Yee, H.K.C., Bechtold, J., & Elston, R. 1996, ApJ, 466, L71

Esteban, C., Peimbert, M., Torres-Peimbert, S., & Escalante, V. 1998, MNRAS, 295, 401

Fedchak, J.A., Wiese, L.M., & Lawler, J.E. 2000, ApJ, 538, 773

Federman, S.R., Glassgold, A.E., & Kwan, J. 1979, ApJ, 227, 466

Feltzing, S., Gilmore, G., & Wyse, R. F. G. 1999, ApJ, 516, L17

Ferland, G. J., Korista, K. T., Verner, D. A., Ferguson, J. W., Kingdon, J. B., & Verner, E. M. 1998, PASP, 110, 761

Frayer, D.T., Papadopoulos, P.P., Bechtold, J., Seaquist, E.R., Yee, H.K.C., & Scoville, N.Z. 1997, AJ, 113, 562

Grevesse, N., & Sauval, A.J. 1998, Space Sci Rev, 85, 161

Heckman, T. M. 2001, in ASP Conf. Ser., Extragalactic Gas at Low Redshift, ed. J. Mulchaey and J. Stocke, (San Francisco: ASP), in press (astro-ph/0107438)

Heckman, T. M., Lehnert, M. D., Strickland, D. K., & Armus, L. 2000, ApJS, 129, 493

Heckman, T. M., Sembach, K. R., Meurer, G. R., Leitherer, C., Calzetti, D., & Martin, C. L. 2001a, ApJ, 558, 56

Heckman, T. M., Sembach, K. R., Meurer, G. R., Strickland, D.K., Martin, C. L., Calzetti, D., & Leitherer, C. 2001b, ApJ, 554, 1021

Henry, R.B.C., Edmunds, M.G., & Köppen, J. 2000, ApJ, 541, 660

Hollenbach, D.J., Werner, M.W., & Salpeter, E.E. 1971, ApJ, 163, 165

Holweger, H. 2001, in Solar and Galactic Composition, ed. R.F. Wimmer-Schweingruber, (Berlin: Springer), in press

Howk, J.C., & Sembach, K.R. 1999, ApJ, 523, L141

Jimenez, R., Bowen, D.V., & Matteucci, F. 1999, ApJ, 514, L83

Jenkins, E.B., et al. 2000, ApJ, 538, L81

Kennicutt, R.C. 1998, in ASP Conf. Ser. 142, The Stellar Initial Mass Function, ed. G. Gilmore & D. Howell (San Francisco: ASP), 1

Kobulnicky, H.A. 1999, in IAU Symposium 193, Wolf-Rayet Phenomena in Massive Stars and Starburst Galaxies, ed. K. A. van der Hucht, G. Koenigsberger, & P.R.J. Eenens, (San Francisco: ASP), 670

Leitherer, C., et al. 1999, ApJS, 123, 3

Leitherer, C., Leão, J. R. S., Heckman, T. M., Lennon, D. J., Pettini, M., & Robert, C. 2001, ApJ, 550, 724

Mar, D.P., & Bailey, G. 1995, PASA, 12, 239

Meyer, D.M., Cardelli, J.A., & Sofia, U.J. 1997, ApJ, 490, L103

Mo, H.J., Mao, S., & White, S.D.M. 1999, MNRAS, 304, 175

Molaro, P., Levshakov, S. A., D'Odorico, S., Bonifacio, P., & Centurión, M. 2001, ApJ, 549, 90

Morton, D.C. 1991, ApJS, 77, 119

Nagamine, K., Fukugita, M., Cen, R., & Ostriker, J.P. 2001, ApJ, 558, 497

Nakanishi, K., Ohta, K., Takeuchi, T. T., Akiyama, M., Yamada, T., & Shioya, Y. 1997, PASJ, 49, 535

Navarro, J. F., Frenk, C. S., & White, S. D. M. 1997, ApJ, 490, 493

Pagel, B.E.J., Edmunds, M.G., Blackwell, D.E., Chun, M.S., & Smith, G. 1979, MNRAS, 189, 95

Papovich, C., Dickinson, M., & Ferguson, H.C. 2001, ApJ, 559, 620

Pettini, M. 1999, in Chemical Evolution from Zero to High Redshift, ESO Astrophysics Symposia, ed. J.R. Walsh & M.R. Rosa, (Berlin: Springer), 233 (astro-ph/9902173)

Pettini, M., Boksenberg, A., & Hunstead, R.W. 1990, ApJ, 348, 48

Pettini, M., Ellison, S.L., Steidel, C.C., & Bowen, D.V. 1999, ApJ, 510, 576

Pettini, M., Ellison, S.L., Steidel, C.C., Shapley, A.E., & Bowen, D.V. 2000b, ApJ, 532, 65

Pettini, M., Shapley, A. E., Steidel, C. C., Cuby, J.G., Dickinson, M., Moorwood, A. F. M., Adelberger, K. L., & Giavalisco, M. 2001, ApJ, 554, 981

Pettini, M., Steidel, C. C., Adelberger, K. L., Dickinson, M., & Giavalisco, M. 2000a, ApJ, 528, 96 (Paper I)

Prochaska, J.X., & Wolfe, A.M. 2002, ApJ, in press (astro-ph/0110351)

Prochaska, J.X., Wolfe, A.M., Tytler, D., Burles, S., Cooke, J., Gawiser, E., Kirkman, D., O'Meara, J.M., & Storrie-Lombardi, L. 2001, ApJS, 137, 21

Savage, B.D., Bohlin, R.C., Drake, J.F., & Budich, W. 1977, ApJ, 216, 291

Savage, B.D., & Sembach, K.R. 1991, ApJ, 379, 245

Savage, B.D., & Sembach, K.R. 1996, ARA&A, 34, 279

Sawicki, M. 2001, AJ, 121, 2405

Seitz, S., Saglia, R.P., Bender, R., Hopp, U., Belloni, P., & Ziegler, B. 1998, MNRAS, 298, 945

Sembach, K.R., Howk, J.C., Ryans, R.S.I., & Keenan, F.P. 2000, ApJ, 528, 310

Sembach, K.R., & Savage, B.D. 1996, ApJ, 457, 211

Shapley, A.E., Steidel, C.C., Adelberger, K.L., Dickinson, M., Giavalisco, M., & Pettini, M. 2001, ApJ, 562, 95

Sheinis, A. I., Miller, J. S., Bolte, M., & Sutin, B. M. 2000, Proc. SPIE, 4008, 522

Sofia, U.J., & Jenkins, E.B. 1998, ApJ, 499, 951

Sofia, U.J., & Meyer, D.M. 2001a, ApJ, 554, L221

Sofia, U.J., & Meyer, D.M. 2001b, ApJ, 558, L147

Songaila, A. 2001, ApJ, 561, L153

Steidel, C.C., Giavalisco, M., Pettini, M., Dickinson, M., & Adelberger, K.L. 1996, ApJ, 462, L17

Steidel, C.C., Pettini, M., & Adelberger, K.L. 2001, ApJ, 546, 665

Steigman, G., Strittmatter, P.A., & Williams, R.E. 1975, ApJ, 198, 575

Strickland, D. K., & Stevens, I.R. 2000, MNRAS, 314, 511

Tenorio-Tagle, G., Silich, S.A., Kunth, D., Terlevich, E., & Terlevich, R. 1999, MNRAS, 309, 332

Teplitz, H. I., McLean, I. S., Becklin, E. E., Figer, D. F., Gilbert, A. M., Graham, J. R., Larkin, J. E., Levenson, N. A., & Wilcox, M. K. 2000, ApJ, 533, L65

Tumlinson, J., et al. 2002, ApJ, in press (astro-ph/0110262)

van der Werf, P.P., Knudsen, K.K., Labbé, I., & Franx, M. 2000, in Deep Millimeter Surveys, ed. J. Lowenthal & D. Hughes, in press (astro-ph/0010459)

Vladilo, G. 1998, ApJ, 493, 583

Vladilo, G., Centurión, M., Bonifacio, P., & Howk, J. C. 2001, ApJ, 557, 1007

Wallerstein, G., & Silk, J. 1971, ApJ, 170, 289

Wolfe, A.M., & Prochaska, J.X. 2000, ApJ, 545, 603

Yee, H.K.C., Ellingson, E., Bechtold, J., Carlberg, R.G., & Cuillandre, J.-C. 1996, AJ, 111, 1783

Table 1. Interstellar Absorption Lines

Ion	$\lambda_{\rm lab}$[a] (Å)	f	$z_{\rm abs}$[b]	Δv[c] (km s^{-1})	W_0[d] (Å)	σ[d] (Å)	Comments
C I	1157.1857	0.5495	2.7241	−475 to + 25	0.18	0.05	
C II	1334.5323	0.1278	2.7245	−775 to +325	3.45	0.04	Blended with C II* λ1335.7.
C IV	1548.204	0.1908	2.7243	−775 to +225	4.17	0.05	W_0 refers to C IV λ1549 *doublet*.[e]
C IV	1550.781	0.09522	2.7245	−775 to +225	4.17	0.05	W_0 refers to C IV λ1549 *doublet*.[e]
N I	1134.1653	0.01342	B	−475 to + 25	1.42	0.07	W_0 refers to N I λ1134 *triplet*.
N I	1134.4149	0.02683	B	−475 to + 25	1.42	0.07	W_0 refers to N I λ1134 *triplet*.
N I	1134.9803	0.04023	B	−475 to + 25	1.42	0.07	W_0 refers to N I λ1134 *triplet*.
N I	1199.5496	0.1328	B	−475 to + 25	2.18	0.04	W_0 refers to N I λ1199 *triplet*.
N I	1200.2233	0.08849	B	−475 to + 25	2.18	0.04	W_0 refers to N I λ1199 *triplet*.
N I	1200.7098	0.04423	B	−475 to + 25	2.18	0.04	W_0 refers to N I λ1199 *triplet*.
N V	1238.821	0.1570	2.7244	−425 to −125	0.23	0.04	
N V	1242.804	0.07823	2.7242	−425 to −125	0.23	0.03	
O I	1302.1685	0.04887	2.7242	−775 to +125	4.25	0.04	W_0 refers to O I λ1302, Si II λ1304 blend.
Mg I	2026.4768	0.1154	B	−475 to + 25	0.57	0.02	W_0 refers to Zn II λ2026, Mg I λ2026 blend.
Mg II	1239.9253	0.00062	B	−350 to −200	0.15	0.03	W_0 refers to Mg II λ1240 *doublet*.
Mg II	1240.3947	0.00035	B	−350 to −200	0.15	0.03	W_0 refers to Mg II λ1240 *doublet*.
Al II	1670.7886	1.833	2.7239	−775 to +125	2.75	0.02	
Al III	1854.71829	0.5602	(2.7244)	−775 to +225	>1.90	>0.03	Partial blend.
Al III	1862.79113	0.2789	2.7239	−775 to +225	1.54	0.03	
Si II	1260.4221	1.007	(2.7238)	−775 to +125	2.80	0.04	Blended with S II λ1259.519.
Si II	1304.3702	0.094	2.7242	−775 to +125	4.25	0.04	W_0 refers to O I λ1302, Si II λ1304 blend.
Si II	1526.70698	0.130	2.7239	−775 to +125	2.59	0.03	
Si II	1808.01288	0.00218	2.7245	−475 to + 25	0.53	0.02	
Si II*	1264.7377	0.9034	2.7234	−775 to + 25	0.78	0.03	
Si II*	1309.2757	0.094	2.7239	−475 to + 25	0.15	0.03	
Si II*	1533.4312	0.130	2.7232	−775 to +125	0.69	0.03	
Si III	1206.500	1.669	2.7242	−775 to +225	3.23	0.06	
Si IV	1393.76018	0.5140	2.7244	−775 to +225	2.16	0.03	
Si IV	1402.77291	0.2553	2.7242	−775 to +225	2.01	0.03	
P II	1152.818	0.2361	(2.7248)	−475 to + 25	>0.22	>0.04	Partial blend (in Lyα forest).
S II	1250.584	0.005453	(2.7244)	−475 to + 25	>0.17	>0.03	Partial blend.
S II	1253.811	0.01088	2.7248	−475 to + 25	0.52	0.03	
Cr II	2062.2361	0.0780	B	−475 to + 25	0.35	0.03	W_0 refers to Cr II λ2062, Zn II λ2062 blend.
Mn II	2576.877	0.3508	2.7245	−475 to + 25	0.38	0.10	
Fe II	1144.9379	0.106	(2.7239)	−775 to +125	>1.20	>0.07	Partial blend (in Lyα forest).
Fe II	1608.45085	0.058	2.7239	−775 to +125	1.30	0.04	
Fe II	2344.2130	0.114	2.7239	−775 to +125	2.99	0.04	
Fe II	2374.4603	0.0313	(2.7241)	−775 to +125	1.94	>0.07	Line affected by bad pixels.
Fe II	2382.7642	0.300	(2.7239)	−775 to +125	3.41	>0.05	Line affected by bad pixels.
Ni II	1317.217	0.07	2.7249	−475 to + 25	0.20	0.03	
Ni II	1370.132	0.0769	2.7241	−475 to + 25	0.24	0.02	Blended with Si IV λ1393 at $z_{\rm abs} = 2.6606$.
Ni II	1703.4119	0.0060	2.7244	−475 to + 25	0.17	0.02	
Ni II	1709.6042	0.0324	2.7247	−475 to + 25	0.33	0.03	
Ni II	1741.5531	0.0427	2.7244	−475 to + 25	0.30	0.02	
Ni II	1751.9157	0.0277	2.7254	−475 to + 25	0.19	0.03	
Zn II	2026.1371	0.489	B	−475 to + 25	0.57[f]	0.02	W_0 refers to Zn II λ2026, Mg I λ2026 blend.
Zn II	2062.6604	0.256	B	−475 to + 25	0.35	0.03	W_0 refers to Cr II λ2062, Zn II λ2062 blend.

[a]Vacuum wavelengths.

[b]Vacuum heliocentric. See note below.

[c]Velocity range for equivalent width measurements relative to $z_{\rm stars} = 2.7276$.

[d]Rest frame equivalent width and 1σ error.

[e]Blended with stellar C IV.

[f]Blended with stellar features.

Notes to Table 1:

The equivalent width errors listed are from counting statistics only and were calculated from the S/N of the data across each absorption line. Systematic errors due to the uncertainty in the continuum placement are more difficult to quantify. In general, trials with different continuum fits showed them to be comparable to the random errors quoted here. The values of $z_{\rm abs}$ were measured from: (i) the centroid wavelength for unblended lines and (ii) the wavelength of maximum optical depth for partially blended lines. Values in brackets are uncertain for the reasons given in the 'Comments' column. 'B' indicates cases where a reliable value $z_{\rm abs}$ could not be measured because of strong blending. For blended lines the velocity range given for the equivalent width measurements refers to *each* line in the blend.

Table 2. Absorption Line Column Densities

Ion	$\lambda_{\rm lab}$[a] (Å)	f	Optical Depth Method Δv[b] (km s^{-1})	Optical Depth Method log $N_{\rm aod}$ (cm^{-2})	Profile Fitting[c] log $N_{\rm pf}$ (cm^{-2})
H I	1215.6701	0.4164	···	···	20.85
C I	1157.1857	0.5495	−475 to + 25	13.55	13.57
N I	1134.1653	0.01342	···	···	15.35
N I	1134.4149	0.02683	···	···	15.35
N I	1134.9803	0.04023	···	···	15.35
Mg II	1239.9253	0.00062	···	···	16.13
Mg II	1240.3947	0.00035	···	···	16.13
Si II	1260.4221	1.007	···	···	15.77
Si II	1304.3702	0.094	···	···	15.77
Si II	1526.70698	0.130	···	···	15.77
Si II	1808.01288	0.00218	−475 to + 25	15.99	15.77
P II	1152.818	0.2361	−475 to + 25	>14.04[d]	14.00
S II	1250.584	0.005453	−475 to + 25	>15.41[e]	15.43
S II	1253.811	0.01088	−475 to + 25	15.63	15.43
Mn II	2576.877	0.3508	−475 to + 25	13.33	13.13
Fe II	1144.9379	0.106	−775 to +125	>15.22[f]	15.00
Fe II	1608.45085	0.058	−775 to +125	15.17	15.00
Fe II	2344.2130	0.114	···	···	15.00
Fe II	2374.4603	0.0313	−775 to +125	15.25[g]	15.00
Fe II	2382.7642	0.300	···	···	15.00
Ni II	1317.217	0.07	−475 to + 25	14.32	14.10
Ni II	1370.132	0.0769	−475 to + 25	<14.34[h]	14.10
Ni II	1709.6042	0.0324	−475 to + 25	<14.63[i]	(14.10)[i]
Ni II	1741.5531	0.0427	−475 to + 25	<14.45[i]	(14.10)[i]
Ni II	1751.9157	0.0277	−475 to + 25	<14.43[i]	(14.10)[i]

[a]Vacuum wavelengths.

[b]Velocity range used for the apparent optical depth method.

[c]Using the parameters $b = 70$ km s^{-1} and $v = -265$ km s^{-1}, except for H I (see Figure 3).

[d]Blended in red wing.

[e]Blended in wings.

[f]Blended in blue wing.

[g]Linearly interpolated across bad pixels.

[h]Blended with an intervening Si IV λ1393 line at $z_{\rm abs} = 2.6606$; the contribution of the latter to the blend was assessed with reference to the weaker member of the Si IV doublet at λ1402.

[i]Blended with stellar features.

Table 3. Interstellar Abundances

Ion	log N (cm^{-2})	log (X/H)	log (X/H)$_\odot$[a]	[X/H]$_{\rm cB58}$[b]
H I	20.85	···	···	···
N I	15.35	−5.50	−4.07	−1.43
Mg II	16.13	−4.72	−4.42	−0.30
Si II	15.99	−4.86	−4.44	−0.42
P II	14.20[c]	−6.65	−6.44	−0.21
S II	15.63	−5.22	−4.80	−0.42
Mn II	13.33	−7.52	−6.47	−1.05
Fe II	15.20	−5.65	−4.50	−1.15
Ni II	14.32	−6.53	−5.75	−0.78

[a]Solar meteoritic abundance scale from Grevesse & Sauval (1998), except N for which we adopt the recent reevaluation of the solar photospheric abundance by Holweger (2001).

[b][X/H]$_{\rm cB58}$ = log (X/H) − log (X/H)$_\odot$.

[c]Corrected by 0.2 dex (see text in §5.1).

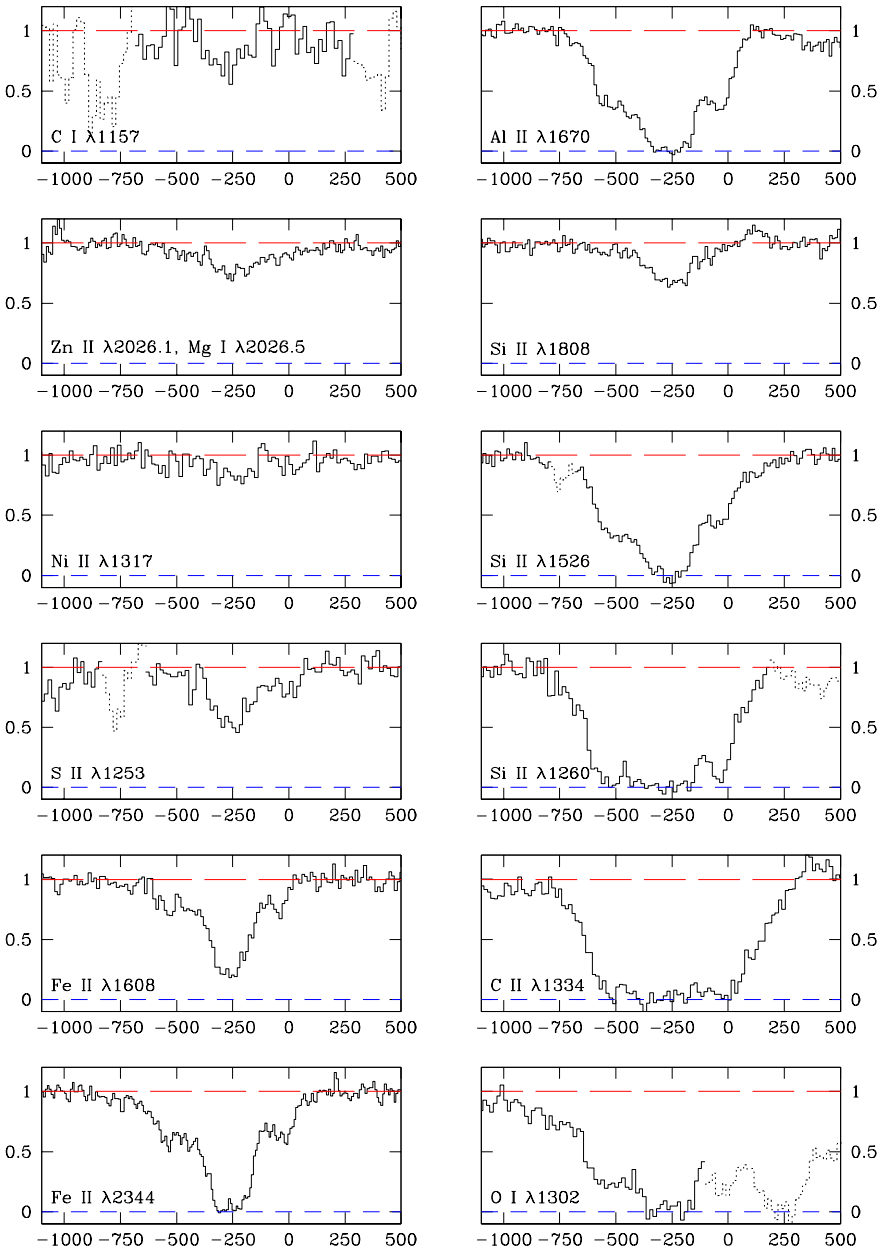

Fig. 1.— Normalised profiles of interstellar absorption lines in cB58. In this figure we have collected examples of absorption lines from species which are the dominant ion stages in H I regions (except for C I), illustrating a range of line strengths. The y-axis is residual intensity, while the x-axis is velocity (in km s^{-1}) relative to the stellar systemic redshift $z_{\rm stars} = 2.7276$ (see §3.1). Each bin corresponds to a wavelength interval $\delta\lambda = 0.067$ Å, equivalent to a velocity interval $\delta v = 8.5$–17.5 km s^{-1} for the transitions shown here. Dotted lines are used to indicate blends with absorption features which are *not* those labelled in each panel.

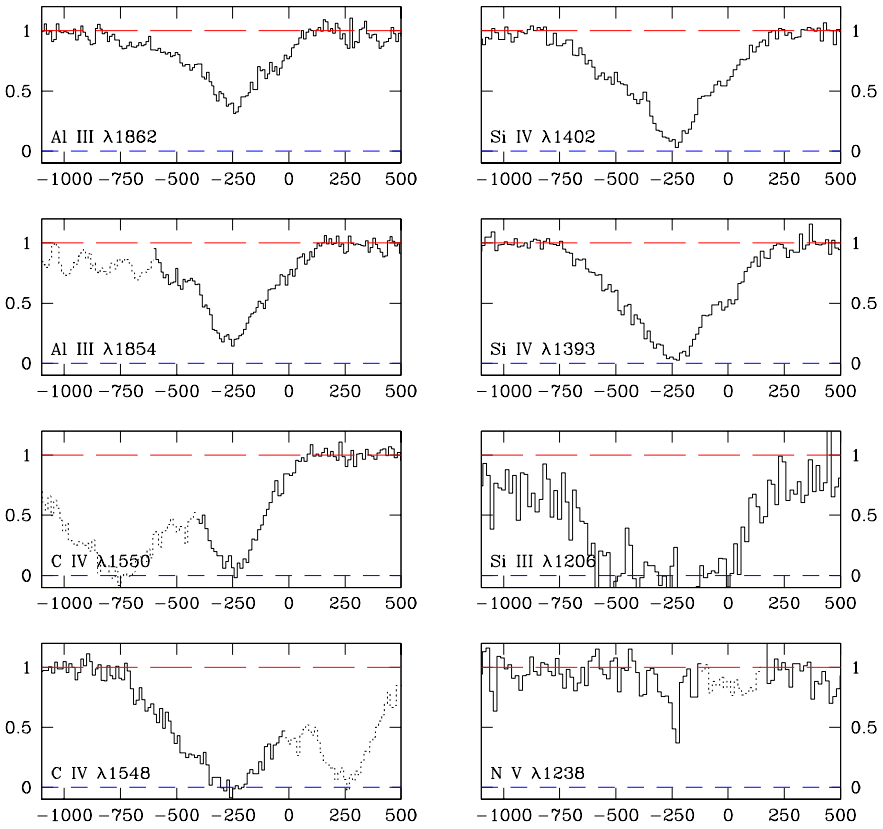

Fig. 2.— Same as Figure 1, showing interstellar absorption line profiles of highly ionized species covered by our ESI spectrum of cB58.

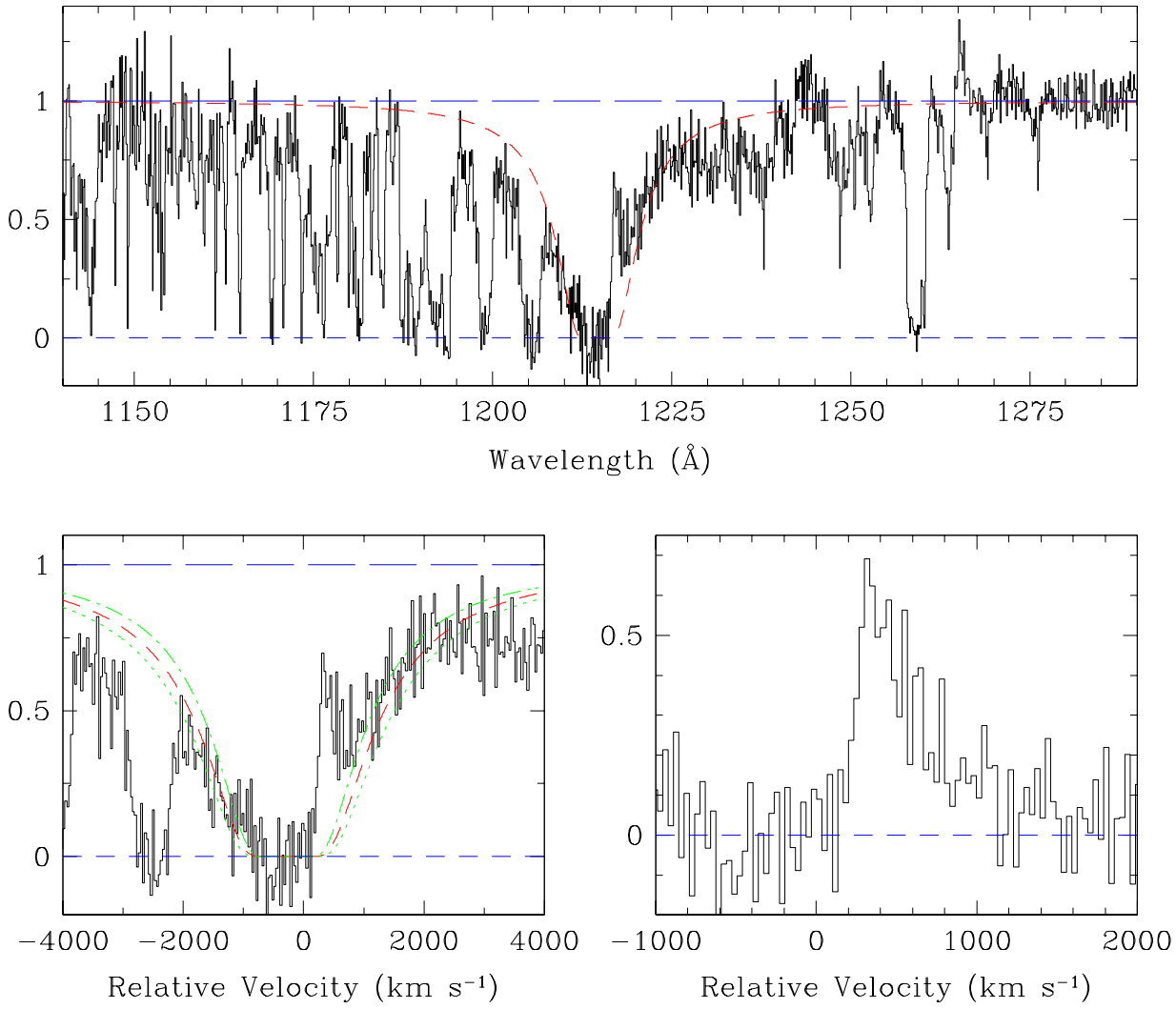

Fig. 3.— The Lyman α profile in cB58. *Top panel*: Black histogram, observed spectrum; dashed line, theoretical absorption profile for N(H I)= 7.0×10^{20} cm^{-2}. *Bottom left-hand panel*: Same as the top panel, but on a velocity scale relative to $z_{\rm stars} = 2.7276$. Also shown are damped profiles for N(H I)= 5.5×10^{20} and 8.5×10^{20} cm^{-2}. *Bottom right-hand panel*: Residual Lyman α emission after subtraction of the N(H I)= 7.0×10^{20} cm^{-2} absorption component. The y-axes of the plots show residual intensity; each bin corresponds to a wavelength interval $\delta\lambda = 0.134$ Å ($\delta v = 33$ km s^{-1}).

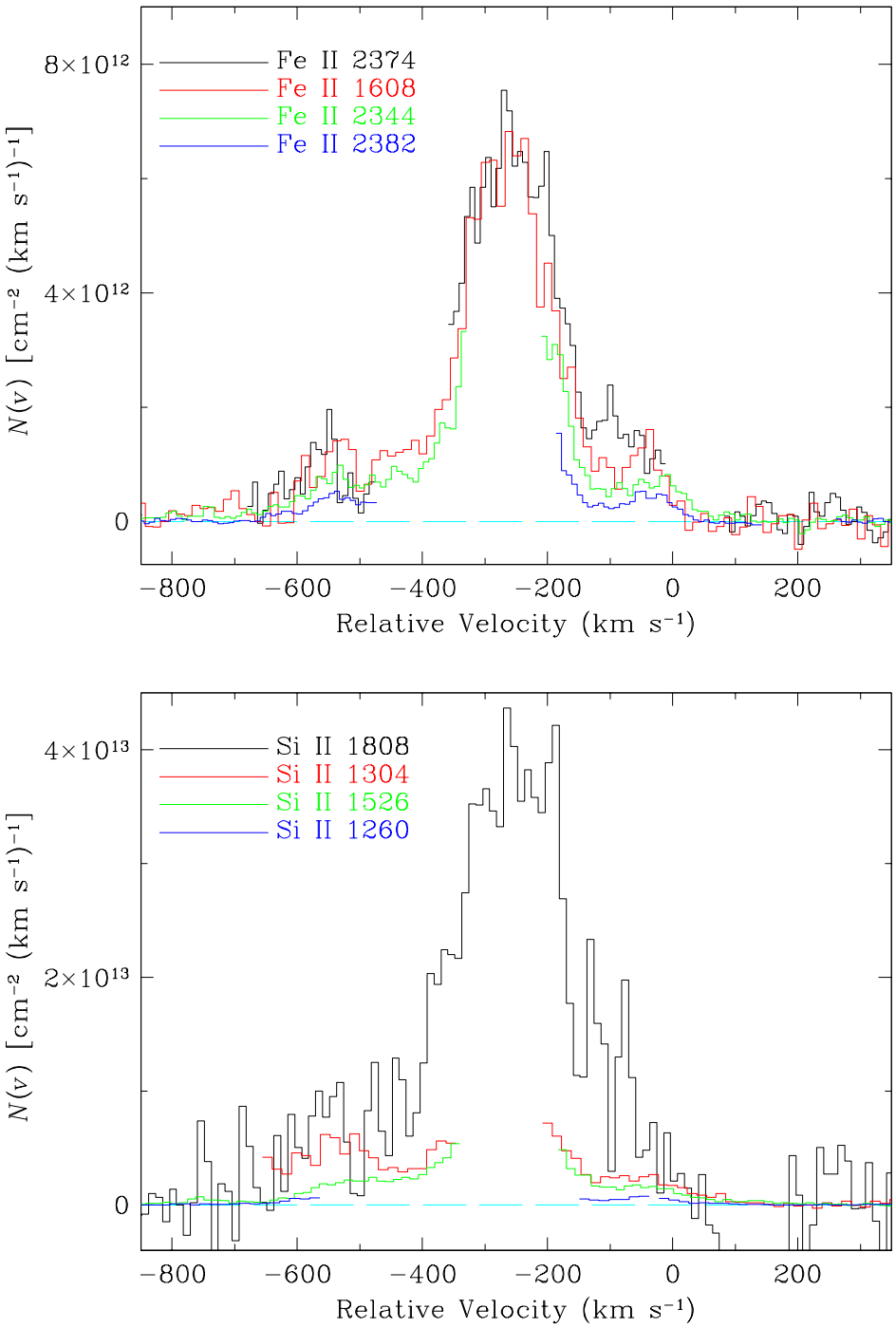

Fig. 4.— Apparent optical depth method: Column density as a function of velocity relative to $z_{\rm stars} = 2.7276$ for Fe II and Si II lines. The transitions are shown in increasing order of $f\lambda$ starting from the top.

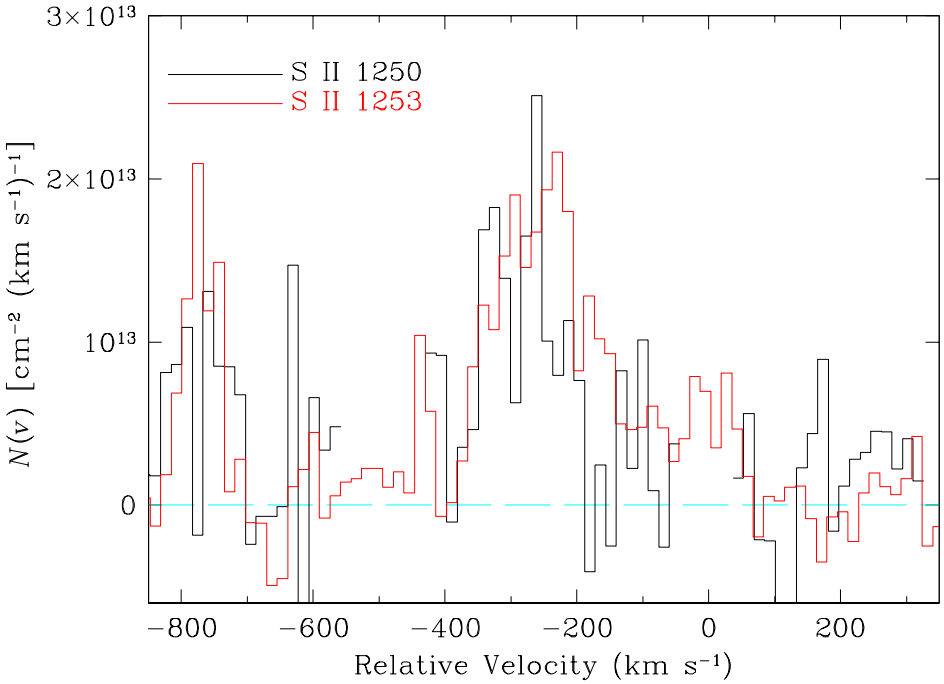

Fig. 5.— Apparent optical depth method: Column density as a function of velocity relative to $z_{\rm stars} = 2.7276$ for two lines of the triplet S II $\lambda\lambda 1250, 1253, 1259$. The products $f\lambda$ for S II $\lambda 1250$ and $\lambda 1253$ respectively are in the ratio 1:2 . The third line, S II $\lambda 1259$, is blended with Si II $\lambda 1260$.

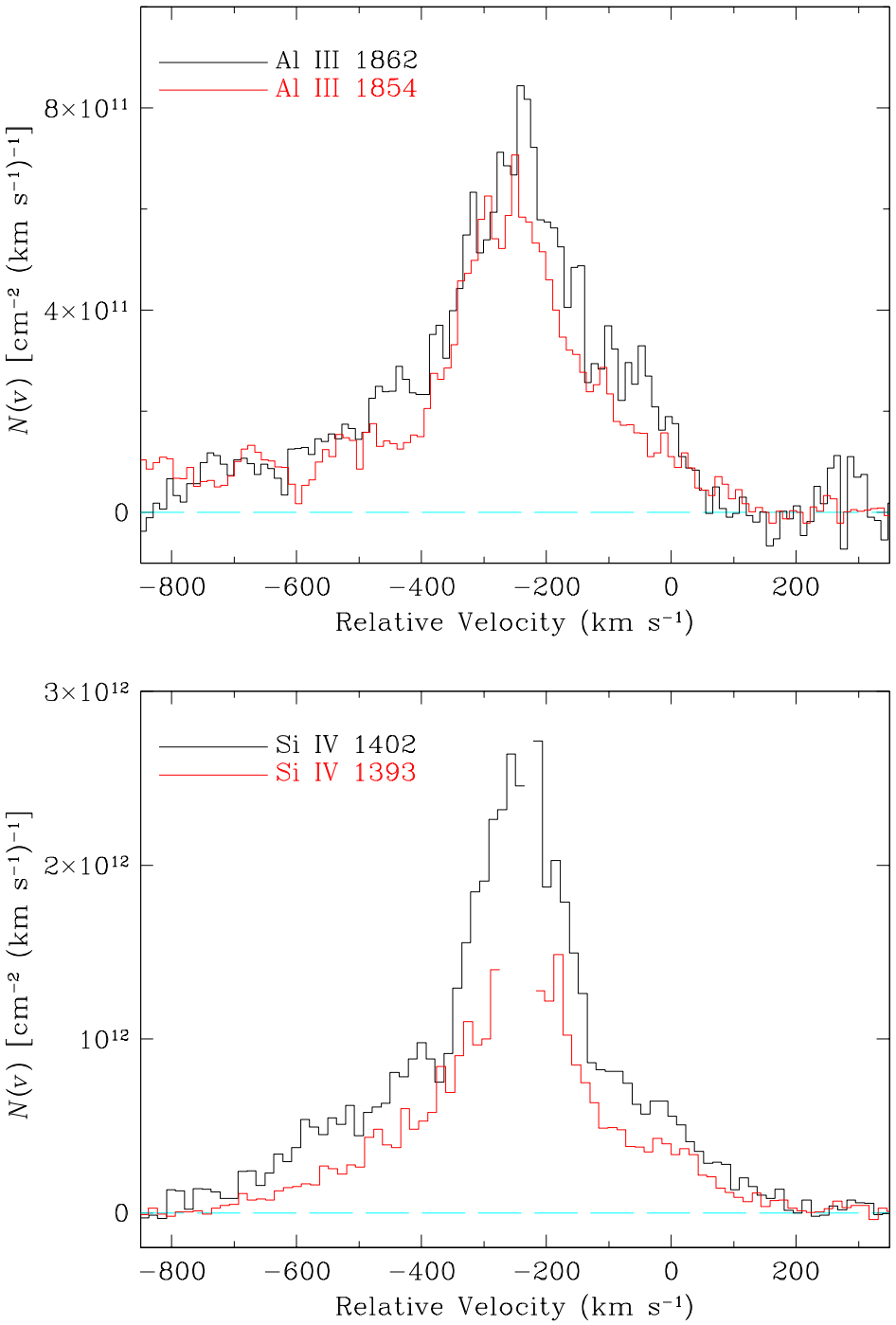

Fig. 6.— Apparent optical depth method: Column density as a function of velocity relative to $z_{\rm stars} = 2.7276$ for the Al III and Si IV doublets. In each case the line at the shorter wavelength is the stronger member of the doublet.

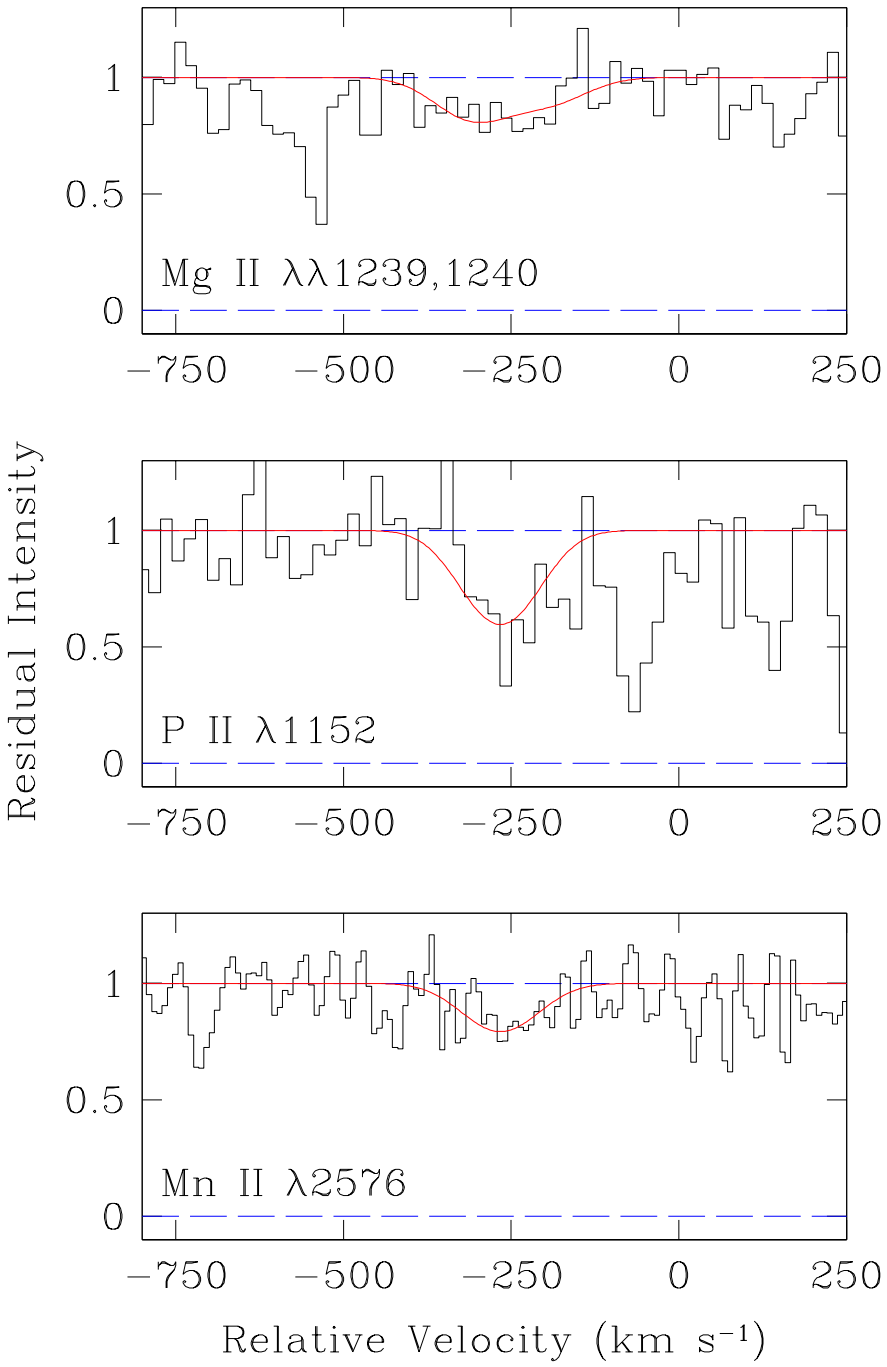

Fig. 7.— Examples of profile fits to weak absorption lines. The fits are for a single absorption component with velocity dispersion parameter $b = 70\,\mathrm{km\ s^{-1}}$ centered at $v = -265\,\mathrm{km\ s^{-1}}$ and convolved with the instrumental broadening profile which is a Gaussian of FWHM = 58 km s^{-1}. The velocity scale is relative to $z_{\mathrm{stars}} = 2.7276$.

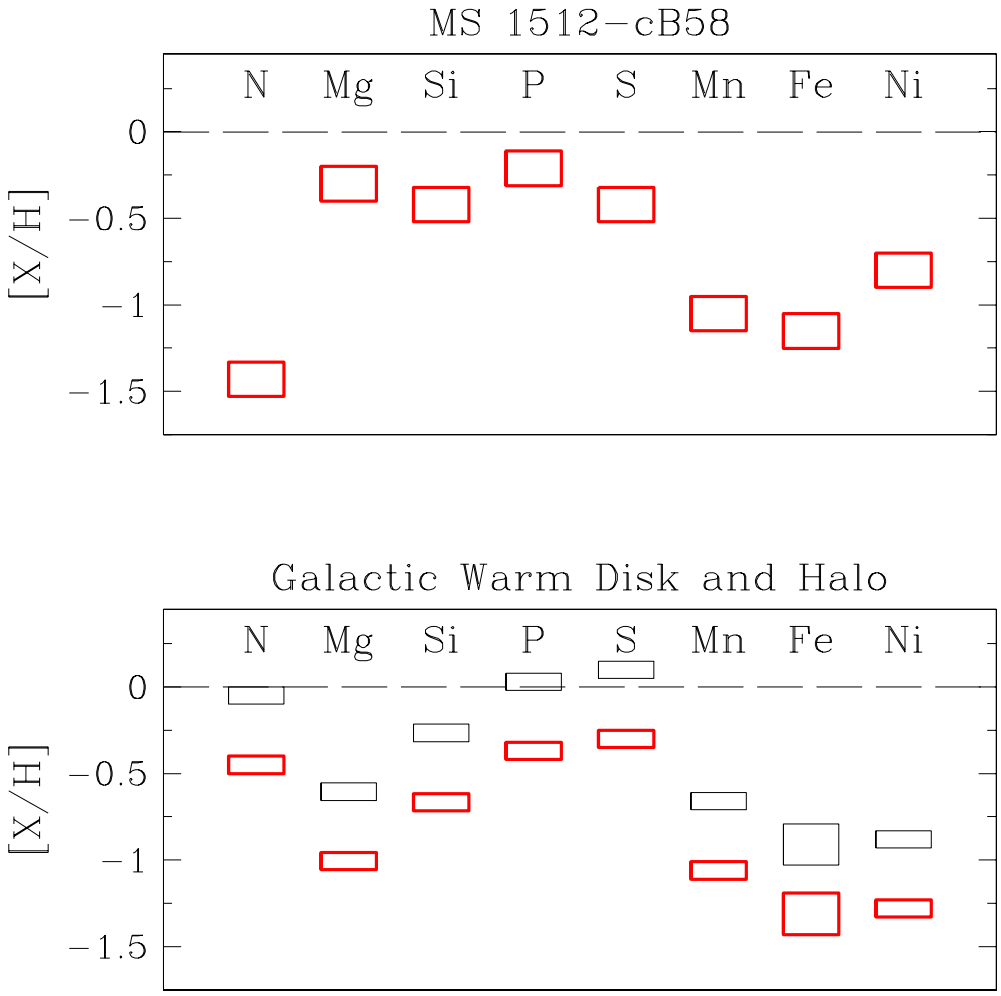

Fig. 8.— *Top Panel:* Element abundances in the interstellar gas of cB58. The height of the boxes reflects the ±0.1 dex statistical uncertainty in the ion column densities; sources of systematic error discussed in the text are expected to be less than about 0.2 dex. *Lower Panel:* The thin boxes show the abundances of the same elements measured in diffuse clouds of the Milky Way (see text for references). The height of the box for Fe reflects the range of abundances among different sight-lines which sample both disk and halo clouds; the same range probably applies to other elements but, in the absence of direct measurements, these boxes have been set to ±0.05 dex. The thick boxes show the same abundance pattern shifted down by 0.4 dex, so as to facilitate the comparison with cB58.

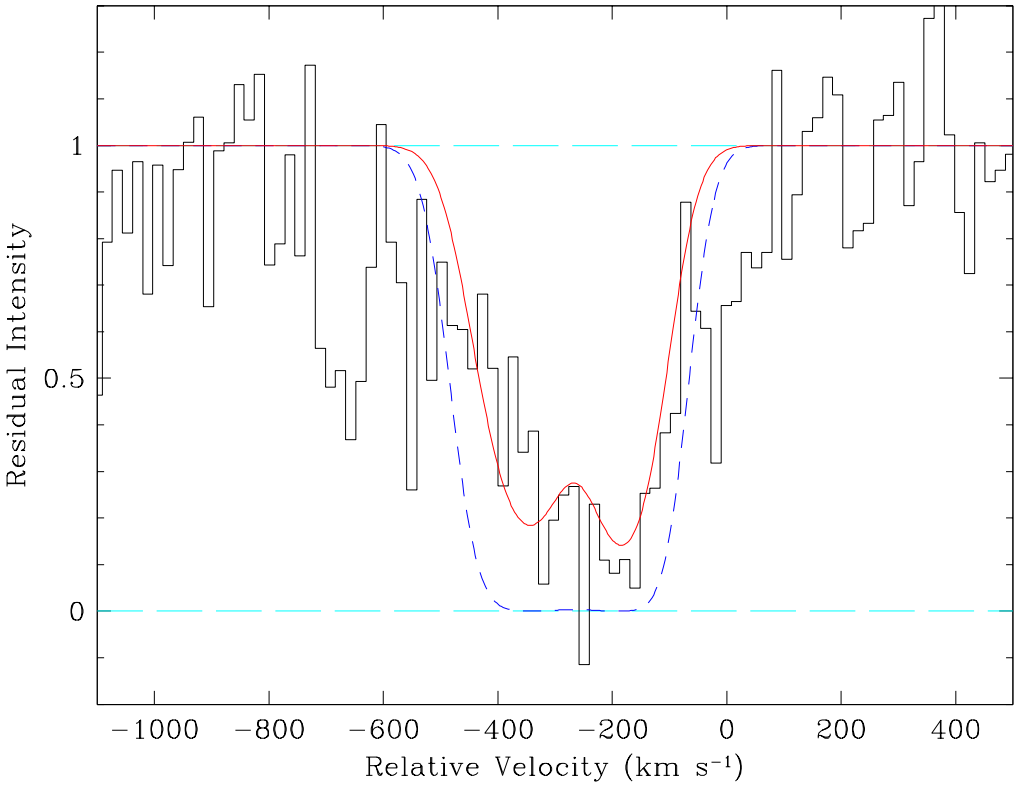

Fig. 9.— The blended N I λ1134 triplet in cB58. The observed profile (histogram) is shown on a velocity scale relative to $z_{\rm stars}$. Also shown are theoretical absorption profiles for the main component of the absorption lines, a single 'cloud' with velocity dispersion parameter $b = 70$ km s^{-1} centered at $v = -265$ km s^{-1}. The continuous line is our best fit, given by a nitrogen column density N(N I) $= 2.2 \times 10^{15}$ cm^{-2}. The dashed line shows the absorption profile corresponding to the nitrogen abundance deduced by Teplitz et al. (2000), which is clearly inconsistent with our data.